REAL-TIME IMAGING AND AUTOMATED SEGMENTATION OF CARTILAGE FROM 2D ULTRASOUND IMAGES.

by

PRAJNA RAMESH DESAI

A thesis submitted to the

School of Graduate Studies

Rutgers, The State University of New Jersey

In partial fulfillment of the requirements

For the degree of

Master of Science

Graduate Program in Biomedical Engineering

Written under the direction of

Ilker Hacihaliloglu

And approved by

_____

_____

_____

New Brunswick, New Jersey

OCTOBER, 2018

ABSTRACT OF THE THESIS

Real-time imaging and automated segmentation of cartilage from 2D ultrasound images.

by Prajna Ramesh Desai

Thesis Director: Ilker Hacihaliloglu

Knee osteoarthritis (OA), a chronic joint condition, occurs when the cartilage cushion between the knee joints degrades over the age. The progression of OA is determined based on the cartilage degradation, therefore, cartilage thickness is an important measure for diagnosis and classification of OA. Currently, magnetic resonance imaging (MRI) is used as the gold standard imaging modality for the diagnosis of OA. However, the routine clinical monitoring using MRI is limited as MRI is expensive, has high scanning time, and limited accessibility. Recently, ultrasound (US) has shown its sensitivity to evaluate the cartilage changes. US provides cost-effective, and real time imaging of knee joint thus making it a potential alternative to MRI for routine clinical monitoring of cartilage degeneration. However, low contrast, speckle noise, signal attenuation, shadow artifacts, and being a user dependent imaging modality have prohibited the widespread use of this imaging modality for diagnosing OA. Various studies have been conducted to show the potential of US for routine clinical monitoring of OA. However, the studies were only focused on qualitative assessment of US cartilage image and the cartilage thickness was computed manually. This thesis, presents a fully automated cartilage segmentation and thickness computation from enhanced 2D US knee cartilage images.

The proposed framework consists of: (1) cartilage image enhancement, (2) bone surface segmentation for seed initialization, (3) seed-based cartilage segmentation, and (4) automatic cartilage thickness measurement. Local phase image features, by designing various bandpass quadrature filters, are extracted for enhancing the cartilage image, and bone surfaces. The segmentation of enhanced bone surfaces is achieved using a dynamic programming approach. The extracted bone surfaces are marked as an initial seeds for region based segmentation algorithms. Cartilage segmentation is evaluated using random walker (RW), watershed, and graph-cut methods. During the final step the segmented cartilage regions are used to compute mean cartilage thickness.

The qualitative and quantitative validations are performed on 200 2D scans obtained from ten healthy volunteers. Validation against expert manual segmentation achieved mean dice similarity coefficient (DSC) of 0.90, 0.86, and 0.84 for RW, watershed, and graph-cut respectively. The computed mean cartilage thickness ranged from 1.90 to 5.66 mm with the average value of 2.95 $\pm$0.66mm. The Bland-Altman plots are used to compare the mean thickness error among different type of segmentation algorithm.

This study presents a, fully automated US cartilage segmentation approach for cartilage segmentation. Presented results show the potential of US for imaging cartilage. The work will be invaluable for all future studies investigating US as an alternative imaging modality in OA research with a specific focus on cartilage.

Acknowledgements

I would like to thank few people without whom this would have not been possible. I would like to express my heartfelt gratitude to my supervisor Dr. Ilker Hacihaliloglu for his constant support, encouragement, and advice during my years at Rutgers University. I have been extremely lucky to have Dr. H as my supervisor who cared so much about the work, for always being there, patiently correcting my mistakes and making me grow as an individual. I would like to thank Dr. Mark Pierce, and Dr. Nada Boustany for dedicating their time to being a part of my thesis committee.

I would like to thank my lab mates especially Cosmas, for being an excellent person and helping me with my silly doubts. Completing this work would have been all the more difficult were it not for the family, friends and World konkani centre(Mangalore), India.

Last but not least, Aayi, Bappa and my lovely sisters thank you for being my strength throughout. I know how much sacrifice and struggle you had to go through so that I could have better education and pursue my dreams. You gave wings to my dreams and let me fly. I know this thank you is not enough for your sacrifices. Love you.

Dev Baren Karon(God bless you all)

Prajna

Table of Contents

Abstract ii

Acknowledgements iv

List of Figures viii

List of Tables xi

1. Introduction 1

1.1. Thesis Motivation 1

1.2. Knee cartilage anatomy 2

1.3. Diagnosis of osteoarthritis 3

1.3.1. X-Ray Radiography 3

1.3.2. Magnetic resonance imaging 4

1.3.3. Optical coherence tomography 5

1.3.4. Ultrasound 6

1.4. Literature review 6

1.5. Problem statement 10

1.6. Objective 12

1.7. Scope of the work 12

References 13

2. Knee imaging using ultrasound, challenges 21

2.1. Bone surface and cartilage appearance in ultrasound 21

2.2. Ultrasound imaging artifacts 21

2.2.1. Speckle noise 22

2.2.2. Bone shadow artifact 24

2.2.3. Manual data collection using hand held ultrasound transducer . 25
2.3. Local phase image features 26
References 28

3. Methods 30
3.1. Cartilage image enhancement 31
3.2. Automated seed initialization 33
3.2.1. Bone feature enhancement 34
3.2.2. Bone shadow enhancement 36
3.2.3. Bone surface extraction 38
3.3. Cartilage segmentation 39
3.3.1. Random walker image segmentation 40
3.3.2. Watershed image segmentation 40
3.3.3. Graph-cut image segmentation 41
3.3.4. Seed initialization 42
3.4. Cartilage thickness measurement 43
3.5. Data Acquisition 45
3.6. Quantitative analysis 46
3.6.1. Dice similarity coefficient 47
3.6.2. Bland-Altman plots 47
References 48

4. Results and Discussion 52
4.1. Cartilage segmentation 52
4.1.1. Cartilage segmentation qualitative results 52
4.1.2. Cartilage segmentation quantitative results 54
4.2. Cartilage thickness computation 58
4.3. Discussion 59
References 63

5. Conclusion and Future work 64

5.1. Conclusion 64

5.2. Limitations 65

5.3. Future work 65

5.3.1. Assessment of degree of cartilage degeneration 65

5.3.2. Assessment of tracked ultrasound volume for increased field of view 66

5.3.3. Assessment of ultrasound image using deep learning segmentation algorithm 66

5.3.4. Comparison of cartilage thickness between ultrasound and magnetic resonance imaging 66

List of publications 67

Appendix 68

Ethics approval letter 68

Elsevier license agreement letter 71

List of Figures

1.1. Knee cartilage anatomy. (a) Cartilage of the knee. (b) OA knee joint . . 2

1.2. US based cartilage degradation grades. Reprinted from [82] with permission from Elsevier. 9

1.3. (a) In vivo US image depicting femoral condylar articular cartilage. (b) Incorrect positioning of US transducer with respect to image plane showing poor image quality. 11

2.1. B-mode knee US image depicting cartilage region (shown with white arrows), femoral bone surface (shown with red arrows) and soft tissue interfaces (shown with yellow arrows). 22

2.2. Speckle appearance in 2D US knee cartilage image for different US machine setting. 23

2.3. B-mode knee US image depicting shadowing (arrows) 25

2.4. US dependency on placement and positioning of transducer by the user: (a) Correct alignment of US transducer. (b) Incorrect alignment of US transducer introducing missing bone boundary denoted by red arrows. . 25

2.5. Importance of phase information. (a) B-mode US image of knee cartilage. (b) B-mode US knee cartilage image acquired by changing the US transducer position. (c) Image reconstructed by phase information from (a), and magnitude from (b). (d) Image reconstructed by phase information from (b), and magnitude from (a). 27

3.1. Flowchart of the proposed method 30

3.2. In vivo US image enhancement: Column (a) In vivo B-mode US image $US(x, y)$. Column (b) Enhanced US image $USE(x, y)$. 33

3.3. Local phase based bone surface enhancement. (a) Input original B-mode US image $US(x, y)$. (b) Enhanced US image $USE(x, y)$. (c) Local phase tensor $LPT(x, y)$ image. (d) Local phase energy $LPE(x, y)$ image. (e) Local weighted mean phase angle $LwPA(x, y)$ image. (f) Local phase $LP(x, y)$ image. 37

3.4. Bone surface segmentation (a) Enhanced bone shadow image BSE(x,y) (low intensity is denoted with blue, and high intensity is denoted with dark red color coding). (b) Bone probability image. (c) Regions showing bone, boneless, and jump. (d) Segmented bone surface overlaid on original B-mode US image 39

3.5. Seed Initialization on enhanced US image (Red: Foreground seeds, Green: background seeds): (a) Foreground and background seeds RW segmentation algorithm. (b) Internal and external markers for watershed algorithm. (c) Foreground and background seeds for graph-cut algorithm. . 43

3.6. Cartilage thickness measurement: (a) Manual thickness measurement using ten anatomical landmarks shown with yellow arrows. (b) Automatically segmented cartilage. (c) Distance map obtained from the segmented image shown in (b), Red pixels denote the cartilage boundary. 44

3.7. Participant setup and US probe positioning. 45

4.1. Qualitative results showing segmented cartilage from enhanced US image: Automatically segmented cartilage overlaid on the manual segmentation (Red: False negative, Cyan: False positive, White: Manually segmented cartilage): (a) Manual segmentation overlaid on RW. (b) Manual segmentation overlaid on watershed. (c) Manual segmentation overlaid on graph-cut. Segmented cartilage region overlaid on original B-mode US: (d) RW segmented cartilage overlaid on B-mode US. (e) Watershed segmented cartilage overlaid on B-mode US. (f) graph-cut segmented cartilage overlaid on B-mode US. 53

4.2. Segmented cartilage region overlaid on original B-mode US: Column (a) original B-mode US image. Column (b) Manually segmented cartilage overlaid on B-mode US. Column (c) RW segmented cartilage overlaid on B-mode US. Column (d) Watershed segmented cartilage overlaid on B-mode US. Column (e) Graph-cut segmented cartilage overlaid on B-mode US. 54

4.3. Qualitative results of cartilage segmentation on original B-mode US: Manual segmented cartilage overlaid on the automatically segmented by using (Red: False negative, Cyan: False positive, White: Manually segmented cartilage): (a) RW. (b) Watershed. (c) Graph-cut. Segmented cartilage region overlaid on original B-mode US: (d) RW segmented cartilage overlaid on B-mode US. (e) Watershed segmented cartilage overlaid on B-mode US. (f) graph-cut segmented cartilage overlaid on B-mode US. 55

4.4. Dice similarity coefficient plots for comparison of segmentation algorithm with respect to manual segmentation. (a) DSC measures for different methods over a set of 200 B-mode US images evaluated using enhanced US images. (b) DSC measures for different methods over a set of 200 B-mode US images evaluated using original B-mode US images. 56

4.5. Example input images with poor DSC results. Top row shows the low contrast input images used in segmenting cartilage. Bottom row shows the enhanced cartilage bone surface used to evaluate segmentation result. 57

4.6. Bland-Altman plots for thickness comparison obtained by manual outline and thickness obtained using segmented cartilage region. 59

4.7. 2D US image enhancement. (a) original B-mode US image. (b) MBORBHE enhanced US image. (c) Proposed local phase based enhanced US image. 61

4.8. Seed Initialization on HE based enhanced US image (Red: Foreground seeds, Green: background seeds): (a) Foreground and background seeds RW segmentation algorithm. (b) Internal and external markers for watershed algorithm. (c) Foreground and background seeds for graph-cut algorithm. 61

List of Tables

1.1. Summary of KL grading system for assessment of OA 4

1.2. Summary of proposed grading system for assessment of US knee cartilage thickness 8

2.1. Speed of sound and acoustic impedance of different tissues and organs . 24

3.1. Summary of decision matrix terms and their definitions 46

4.1. Quantitative analysis using enhanced B-mode US images as the input to the segmentation methods. 56

4.2. Quantitative analysis using original B-mode US images as the input to the segmentation methods. 57

4.3. Cartilage thickness measurement. 58

Chapter 1

Introduction

1.1 Thesis Motivation

Knee osteoarthritis (OA), the most common wear and tear disease of the knee joint [1,2], occurs when the cartilage between the joint degrades due to various reasons such as growing age, obesity, inflammation [3], gender, race/ethnicity [4], physical activity, bone density, joint laxity, genetics [5–7], or metabolic syndromes [8]. OA is classified as primary or secondary based on the stage of joint damage. Primary OA occurs without any cause whereas secondary OA occurs due to trauma, infection or metabolic changes. Globally, OA is ranked fifth among all the disabilities [9] affecting approximately 10 percent of population over 60 years of age [10, 11]. In the United States around 30.8 million adults are suffering due to OA [12–17]. Knee OA is also associated with and increased number of other chronic conditions such as obesity (90%), depression(30%), hypertension(40%), and diabetes(15%) [18, 19].

In addition to affecting the quality of life, OA has been a major economic burden on people [13, 20–22]. Study [23], has reported that OA was the major cause of work loss and affected more than 20 million individuals costing more than $100 billion annually to the United States economy. OA results in more than 25% of health care visits contributing more than $27 billion in health care expenditures annually [15, 21]. Eventually, most of the OA patients, around 54% of require total knee replacement (TKR) and the rate of TKR procedures in United States has doubled for overall population and tripled for individuals aged between 45 to 64 [24]. The average cost of a TKR procedure ranges from $20,293 to $26,388 [20].

1.2 Knee cartilage anatomy

The knee joint is covered with white, smooth, fibrous connective tissue cartilage know as articular cartilage which covers the bone and protects the bone surface from rubbing each other and gives mechanical support the knee joint. The articular cartilage covers ends of the femur, the top of the tibia, and the back of the patella. The medial meniscus and lateral meniscus which are attached to the tibia from inside and outside of the knee respectively acts as the shock absorbent cushions. Figure 1.1a shows the cartilage of the knee (the figures were generated using https://mindthegraph.com/).

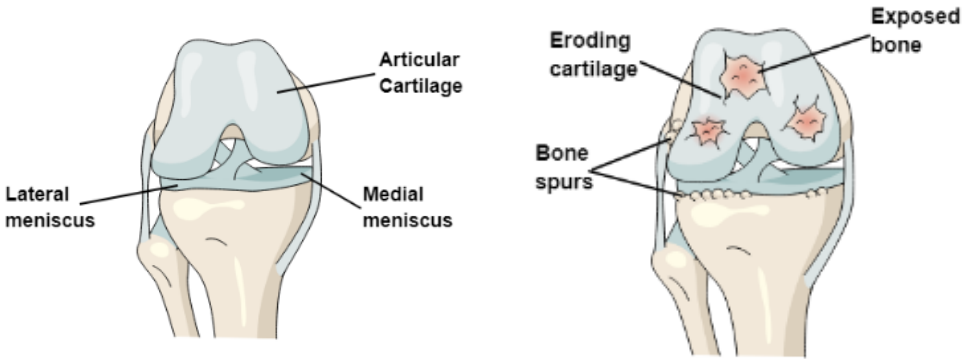

(a) (b)

Figure 1.1: Knee cartilage anatomy. (a) Cartilage of the knee. (b) OA knee joint

The cartilage degradation occurs at the articulating surface and spreads to subchondral space. The degradation leads to the clustering, and clonal expansion of chondrocytes, osteophyte formation or bone spur formation around the joints. The cartilage loss results in pain which can arise from diseased tissue joint, synovium or from articular structure, functional limitation, and affecting the quality of life. The affected articular cartilage produces nerve growth factors that sensitizes local pain fibers resulting in chronic pain. Figure 1.1b shows the OA knee joint with degraded articular cartilage and bone spurs.

The OA can be treated using pharmacological interventions, supportive or educational intervention, non-pharmacological interventions, and surgical interventions. The

surgical intervention includes microfacture, chondrocyte implantation, arthroscopy and debridement, joint replacement, joint fusion, or using soft tissue grafts [25, 26].

1.3 Diagnosis of osteoarthritis

Early diagnosis of OA is very important for better understanding of disease progression and planning for treatment. This section will review various imaging modalities available for OA diagnosis and monitoring. Traditionally, OA has been diagnosed using planar X-ray radiography by measuring narrowing of the joint space width (JSW), or visualizing osteophyte [27,28]. Recent development in other imaging modalities such as magnetic resonance imaging (MRI), ultrasound (US), and optical coherence tomography (OCT) have enhanced OA diagnosis and management through better visualization of cartilage-bone interface and soft tissue depiction.

1.3.1 X-Ray Radiography

X-ray radiographs are used to understand the structural changes and disease progression in routine clinical practice [27–31]. The knee joint is imaged using extended knee that is bilateral antero-posterior image with weight bearing on both knees in full extension. But due to lack of reproducibility, recently a new approach has been proposed where the radiographs are acquired using various degree of knee flexion for better visualization of intra-articular cartilage [32, 33]. Bony features, osteophyte formation, subchondral sclerosis, and cysts can be visualized from collected radiographic data. Evaluation of the joint space width (JSW) is obtained using these anatomical features. Osteophyte and joint space narrowing (JSN) are the two important consideration for assessment of OA. The early phase of OA is predicted using osteophyte whereas severity of OA is assessed using JSN.

The severity of OA is estimated using Kellgren-Lawrence (KL) grading system [34–37]. KL classifies each radiographs into one of five grades ranging from 0 to 4 as none to severe. The KL grade of 0, depicts normal knee with no radiographic features of OA whereas, grade 1 is defined as doubtful JSN but possible osteophyte. Grade 2

indicates definite osteophyte and possible JSN. Multiple osteophyte, definite JSN, bone deformity, and sclerosis forms grade 3, and grade 4 is defined by large osteophyte, marked JSN, and severe sclerosis. Table 1.1 summarizes the KL grading system for the assessment of knee OA.

Table 1.1: Summary of KL grading system for assessment of OA

KL Grade	Complexity	Definition
0	None	No changes
1	Doubtful	Doubtful JSN and possible osteophyte
2	Minimal	Definite osteophyte and possible JSN
3	Moderate	Multiple osteophyte, definite JSN sclerosis, and possible bone deformation
4	Severe	Large osteophyte, severe JSN, and sclerosis definite bone deformation

Traditionally, JSW is computed using manual methods but recent studies are focused on semiautomatic and automated evaluation of JSW [30, 38]. The KL grading system is limited due to linear changes appearing over the period of time. The shortcoming of using X-ray is that it is insensitive to the cartilage degradation, and lacks the soft tissue depiction. In [39], it was shown that significant number of individuals had cartilage loss diagnosed on MRI scans even though there was no prominent JSN using radiographs. The study showed that radiographic progression was 91% specific but only 23% sensitive to the cartilage loss. [39]. Finally, being exposed to ionizing radiation is also another important healthy consideration for X-ray imaging.

1.3.2 Magnetic resonance imaging

Currently, MRI is used as the gold standard for early detection of knee OA. The study [39], showed the prominence of MRI over radiographic assessment. MR images are useful in both morphological and pathological evaluation of OA. Various MR imaging techniques are used to visualize cartilage such as spin echo (SE), fast-spin echo (FSE),

fat suspension or suppressed technique, 2D proton density-weighted or T2 weighted fat suppressed FSE based on the contrast of the image, and Delayed Gadolinium-Enhanced MRI (dGEMRIC) [40–46]. 2D proton density-weighted techniques is widely used in clinical setting to achieve higher contrast between cartilage and subchondral bone [43]. The progression of OA is evaluated using various factors like changes in subchondral bone composition, bone marrow edema like lesion (BML's), subchondral cysts , subchondral bone attrition, and cartilage integrity [47–50]. Various studies have shown the correlation between BML's and OA progression [51–53] and subchondral bone attrition is found in individuals with advanced or severe OA.

The quantitative assessment of cartilage is computed using cartilage volume but its shown that the volume alone could not differentiate between healthy and diseased cartilage as individuals with large bones have larger cartilage volume. Therefore, cartilage thickness is used to evaluate disease progression. Various semiautomatic and automatic frameworks are proposed to segment the cartilage region and compute the thickness from MR images [54–57]. Several semi quantitative morphological grading system such as whole organ MRI score [58], knee OA scoring system [59], and Boston Leeds OA knee scores [60] are used to evaluate knee joint. Even though MRI has shown its validity for disease progression, its use in routine clinical monitoring is limited as getting MRI scan is expensive which costs around $2000 to $3000 for a scan, high scanning time, no real time evaluation, and limited accessibility.

1.3.3 Optical coherence tomography

Recently, OCT has shown its validity for diagnosis of OA [61–64]. OCT is a novel imaging technology which is capable of near real time acquisition of image at high resolution of 4-15 μm. OCT is incorporated with arthroscopes to generate cross-sectional images of articular cartilage. The OCT cartilage evaluation is associated with the collagen orientation. Normal articular cartilage exhibits birefringence that can be detected using light microscopy due to collagen orientation. A healthy cartilage is sensitive to the polarization of incident light of OCT and thus the cartilage birefringence could

be evaluated using this property. The studies [61, 64] have shown that OCT is sensitive to the collagen structural changes caused due to degradation. Loss of polarization and collagen disorientation are important markers that are observed prior to cartilage degradation and fibrillation. The main limitation of using OCT is its invasive procedure required to access the cartilage surface and high user dependency.

1.3.4 Ultrasound

Recently, US has shown its validity to detect the cartilage degradation [65–73] making it possible alternative imaging for the routine clinical monitoring of knee OA. The study [74–76] showed that US is capable of detecting synovial pathologies such as hypertrophy, presence of synovial fluid, and vascularity. US allows non-invasive evaluation of cartilage with higher sensitivity and specificity compared to X-ray radiography [77]. In [78], the results showed that knee synovitis detected by US was correlated with advanced radiographic OA.

Compared to radiography, US lacks ionizing radiations, can be used for multi-planar image acquisition, is portable, easily accessible, allows dynamic assessment of moving structure with real time data analysis, and less expensive as compared to other imaging modalities [67]. The important benefit of using US over radiography includes detection of soft-tissue structure and potential to detect small structural lesions [67, 68]. US is able to evaluate patella-femoral joint including Hoffa pad and anterior femoral surface, periatricular cyst lesions, medial, and lateral joint line which depicts osteophytes and the meniscus. The literature review on validity of US for early detection of knee OA is presented in next section.

1.4 Literature review

Various studies have showed the validity of US for the measurement of cartilage thickness for the early diagnosis of knee OA [79–86]. The studies focused on comparing US data with that of MRI and tried to analyze the sensitivity and accuracy of US to detect the cartilage changes.

The study conducted by Kazam and his team [79], investigated the validity of US femoral cartilage thickness evaluation for routine clinical monitoring of OA. For the study, the 2D femoral articular cartilage were acquired from 20 OA knee (6 women, and 3 men), and 20 healthy knee (7 women, and 3 men). The cartilage thickness were computed manually drawing a line between the cartilage bone interface and the synovial space on original B-mode US images from lateral, central and medial cartilage regions over the duration of three months. The 2D US images were evaluated for cartilage visualization, grading, presence or absence of cartilage calcification, and presence of bony irregularities. The obtained results showed the US can be used as an alternative imaging modality for MRI to identify abnormalities in patients with knee pain.

In [81], Schmitz and his colleagues, conducted a study to understand the relationship between MRI and US in the medial femoral condyle region. For this study, the mean cartilage thickness were measured from left medial femoral cartilage via T1 weighted MRI images. US scans were acquired from left knee using 10 MHz linear transducer with knee placed in 90deg of flexion to acquire cartilage images from transverse, anterior, posterior, and middle medial femoral regions. Ten healthy women and nine healthy men with height, body weight, and age ranging from 1.66 to 1.8 m, 59.5 to 79.1 kg, 21.6 to 21.7 among women and men respectively were enrolled in the study. The results from this study indicated that the cartilage thickness measured manually from drawing line between bone surface and cartilage interface from transverse US were positively correlated with posterior and MRI measurements. The middle and posterior longitudinal US measures were correlated with their respective MRI regions. The results showed the potential and validity of US as a viable clinical tool to assess the relative cartilage thickness from medial and posterior medial femoral regions.

The study conducted by Saarakkala and colleagues [82], focused on investigating the diagnostic performance of US to detect and grade the changes of articular cartilage using arthroscopic as the gold standard. For the study, the knee scan was performed on forty adult patients with knee fully flexed at 120deg from medial and lateral femoral condyle, and the sulcus of femoral condyle followed by knee arthroscopy. The manually measured cartilage thickness were marked based on the grading system generated based on the

cartilage degradation. Table 1.2 refers to the grading standard used to characterize the OA condition as normal to severe. Reported sensitivity, positive and negative predictive values were 83%, 88-100%, and 24-46% respectively. The specificity measurements were greatly significant at femoral sulcus and lateral condyle. The results indicated that the correlation of severe grade cartilage changes between US and arthroscopy varied from significant to insignificant. There was high correlation value at sulcus region followed by medial and lateral condyle. The study concludes that US is a strong indicator for cartilage degeneration and is a promising technique that can be used for screening the degenerating cartilage thickness. Figure 1.2 shows the various US images with the proposed grading condition.

Table 1.2: Summary of proposed grading system for assessment of US knee cartilage thickness

Grade	Complexity	Definition
0	Normal	US shows a sharp hyperechoic anterior and posterior interface
1	Mild degenerative changes	Loss of normal sharpness of cartilage interface
2A	Moderate degenerative changes	Less than 50% loss of cartilage causing local thinning
2B	Moderate	More than 50% but less than 100% loss of cartilage causing local thinning
3	Severe	100% local loss of cartilage tissue

Harkey and colleagues [83], focused their study to determine the magnitude of medial femoral cartilage deformation detected by US followed by walking, and running in twenty-five healthy individuals. For the study, medial femoral cartilage thickness were

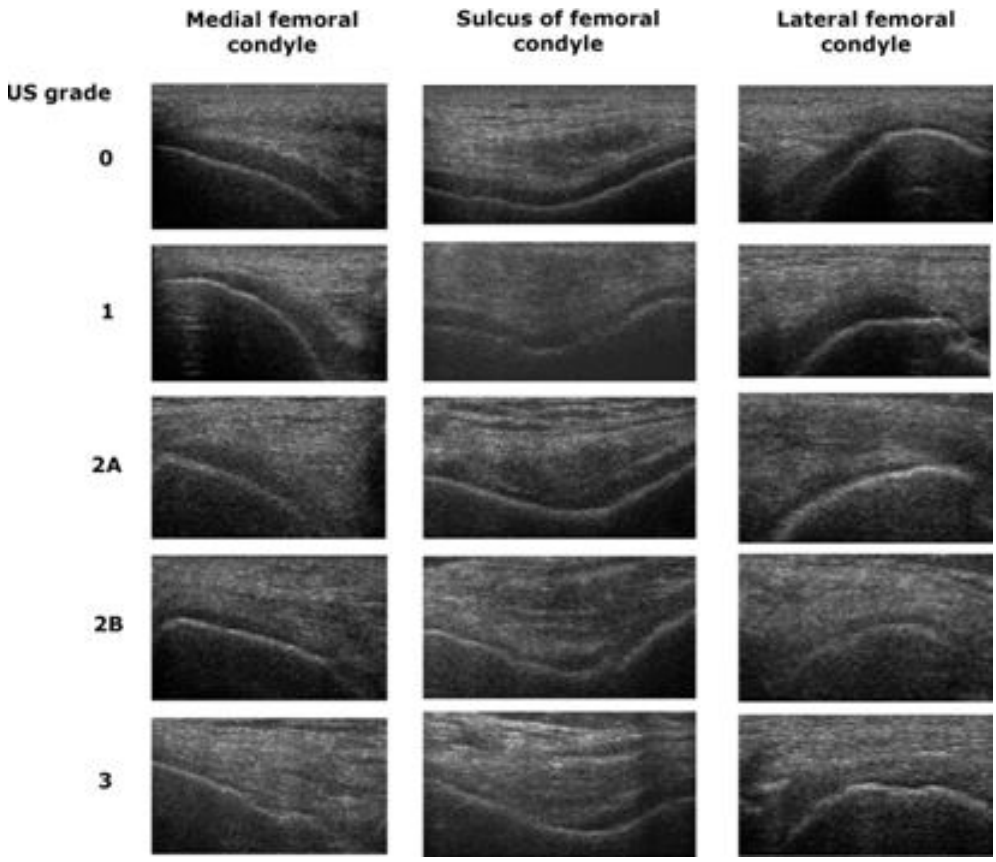

Figure 1.2: US based cartilage degradation grades. Reprinted from [82] with permission from Elsevier.

measured manually before and after three separate thirty minute loading conditions that were conducted on different days separated by one week. In controlled condition, the subject was asked to remain seated for thirty minutes in a long sit position with knee flexed at 140deg. For running and walking, the subjects ran/walked on treadmill at self selected speed for thirty minutes. The cartilage deformation were computed as a percentage change from pre to post loading condition in each case. The result indicated that the deformation was evident between loaded condition i.e., after running and walking compared to controlled condition. These measured thickness demonstrated the sensitivity and reliability of US imaging modality for quantifying cartilage deformation.

The most recent studies are focused on enhancement and automated segmentation of US knee cartilage for better assessment of cartilage thickness. Hossain and colleagues [84], proposed a new histogram equalization (HE) method, multipurpose beta

optimized recursive bi-histogram equalization (MBORBHE), for contrast enhancement of US knee cartilage scans. The advantage of proposed method is that, it considers three different aspects such as brightness, contrast, and preservation of details whereas the traditional HE methods consider only contrast in order to minimize the artifacts for better visualization of the image. The aim of proposed enhancement method is to detect the separation point for segmenting histogram to achieve better brightness and preserve the details of the image. The qualitative and quantitative analyses were done using signal to noise ratio (SNR = 12.37 dB), structure similarity index measurement (0.8735), entropy (5.8831), and mean shift (mean value almost equal to original image value) on scans acquired from twenty healthy subjects.

In [85], Faisal and team proposed a new segmentation and thickness computational approach for 2D US knee cartilage. The locally statistical level set method (LSLSM) was applied to locate the cartilage boundary to segment the cartilage region. The segmentation results were validated with other level set methods such as local Gaussian distribution fitting (LGDF) model, and locally weighted K-means variational level set (WKVLS). The normal distance method was used to measure the cartilage thickness. For the study, the US images were acquired from ten healthy subjects placing knee in supine position fully flexed at 120deg. The qualitative and quantitative analysis was computed on 80 data sets. The qualitative results indicate significant agreement with Cohen's κ coefficient of 0.73. The quantitative assessments were computed using DSC and Hausdorff distance and average values of 0.91±0.01, and 6.21±0.59 was achieved respectively. The measured average cartilage thickness ranged from 1.35 to 2.42 mm. The results indicated the robustness of LSLSM method for cartilage segmentation but it includes two user interactions for initial contour initialization for cartilage boundary detection and extraction of cartilage regions from the surrounding soft tissue.

1.5 Problem statement

The degeneration of cartilage is observed as, the changes in cartilage thickness over the time. Therefore, segmentation is necessary task to provide direct and accurate measure of cartilage thickness from 2D US knee cartilage. Figure 1.3.a shows the

femoral condylar cartilage region in US image which is depicted as a hypoechoic band between cartilage bone interface and cartilage-soft tissue interface. Segmenting the cartilage region from the 2D US knee cartilage image is difficult due to the presence of surrounding soft tissues.

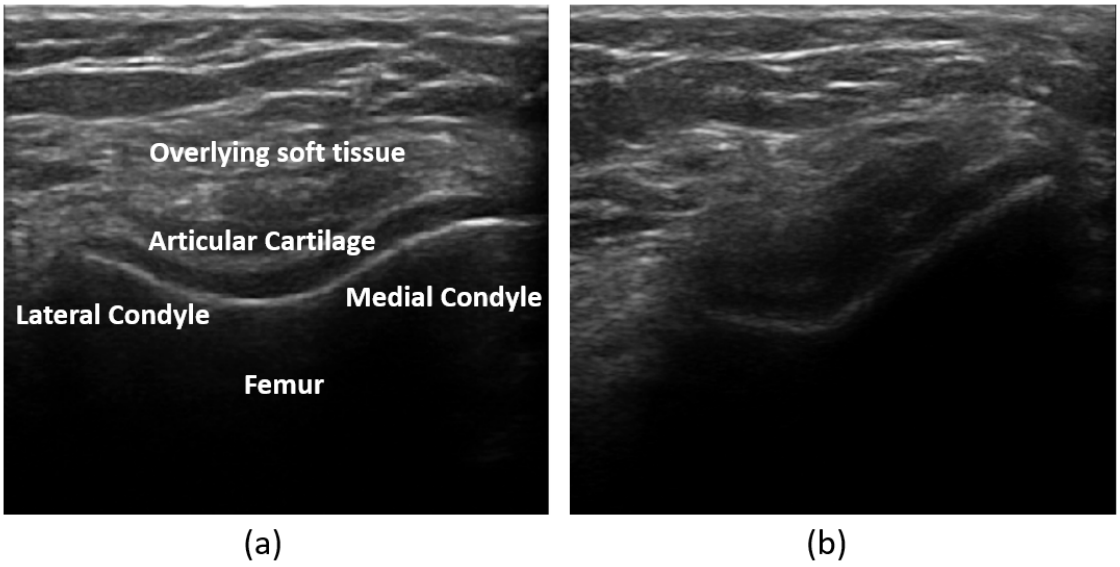

Figure 1.3: (a) In vivo US image depicting femoral condylar articular cartilage. (b) Incorrect positioning of US transducer with respect to image plane showing poor image quality.

Furthermore, due to user dependability of US while acquiring the scans (1.3.b), speckle noise and intensity in homogeneity occurs in the acquired image. The low contrast and speckle noise reduces the image quality, and image interpretation thus complicating the segmentation process in the 2D US knee cartilage images.

Due to these limitations, US has not become a standard of care imaging modality for cartilage imaging for diagnosis of OA. Robust and accurate computational methods are required in order to extract the clinically important features from the collected US data.

1.6 Objective

The main objective of this thesis is to develop fully automated 2D US knee cartilage segmentation methods as an initial step for screening and quantification of cartilage degeneration. Ultimately our research is intended to advance the larger goal of developing a framework where 2D and 3D ultrasound can be used of diagnosis and monitoring of OA in the knee region.

The specific aims of thesis are listed below:

1. To develop an intensity invariant image enhancement method to address the low contrast and speckle noise in 2D US knee cartilage images.
2. To develop a fully automated cartilage US image segmentation and thickness computation method.

These outcomes achieved in this work will help us in the future design, development, and evaluation of a US-based cartilage degeneration system which could provide a potential alternative to MRI as an initial screening method.

1.7 Scope of the work

The scope of this work includes:

1. The enhancement, segmentation, and thickness computation of the knee cartilage are performed in 2D US image.
2. The performance of the presented method are validated using qualitative and quantitative evaluation metrics.
3. The performance of the presented method is compared to other existing methods in the attempt of enhancement and segmentation of the 2D US knee cartilage.

References

[1] Reva C Lawrence, David T Felson, Charles G Helmick, Lesley M Arnold, Hyon Choi, Richard A Deyo, Sherine Gabriel, Rosemarie Hirsch, Marc C Hochberg, Gene G Hunder, et al., "Estimates of the prevalence of arthritis and other rheumatic conditions in the united states: Part ii," *Arthritis & Rheumatism*, vol. 58, no. 1, pp. 26–35, 2008.

[2] G Nuki, "Osteoarthritis: a problem of joint failure," *Zeitschrift für Rheumatologie*, vol. 58, no. 3, pp. 142–147, 1999.

[3] Thomas Aigner, P Van der Kraan, and W Van den Berg, "Osteoarthritis and inflammation-inflammatory changes in osteoarthritic synoviopathy," *Biomedical and health research-commission of the European communities then IOS press*, vol. 70, pp. 219, 2007.

[4] Ana M Valdes, John Loughlin, Mark Van Oene, Kay Chapman, Gabriela L Surdulescu, Michael Doherty, and Tim D Spector, "Sex and ethnic differences in the association of aspn, calm1, col2a1, comp, and frzb with genetic susceptibility to osteoarthritis of the knee," *Arthritis & Rheumatism*, vol. 56, no. 1, pp. 137–146, 2007.

[5] Sophie Catriona Warner and Ana Maria Valdes, "The genetics of osteoarthritis: A review," *Journal of Functional Morphology and Kinesiology*, vol. 1, no. 1, pp. 140–153, 2016.

[6] Yasuhiro Ishidou, Kanehiro Matsuyama, Daisuke Sakuma, Takao Setoguchi, Satoshi Nagano, Ichiro Kawamura, Shingo Maeda, and Setsuro Komiya, "Osteoarthritis of the hip joint in elderly patients is most commonly atrophic, with low parameters of acetabular dysplasia and possible involvement of osteoporosis," *Archives of osteoporosis*, vol. 12, no. 1, pp. 30, 2017.

[7] N Clement, "Is osteoarthritis of the knee hereditary," *A review of the literature. Hereditary Genet*, vol. 1, pp. 2161–1041, 2013.

[8] Peter R Kornaat, Ruby Sharma, Rob J van der Geest, Hildo J Lamb, Margreet Kloppenburg, Marie-pierre Hellio Le Graverand, Johan L Bloem, and Iain Watt, "Positive association between increased popliteal artery vessel wall thickness and generalized osteoarthritis: is oa also part of the metabolic syndrome?," *Skeletal radiology*, vol. 38, no. 12, pp. 1147, 2009.

[9] Christopher JL Murray, Theo Vos, Rafael Lozano, Mohsen Naghavi, Abraham D Flaxman, Catherine Michaud, Majid Ezzati, Kenji Shibuya, Joshua A Salomon, Safa Abdalla, et al., "Disability-adjusted life years (dalys) for 291 diseases and injuries in 21 regions, 1990–2010: a systematic analysis for the global burden of disease study 2010," *The lancet*, vol. 380, no. 9859, pp. 2197–2223, 2012.

[10] D Pereira, B Peleteiro, J Araujo, J Branco, RA Santos, and E Ramos, "The effect of osteoarthritis definition on prevalence and incidence estimates: a systematic review," *Osteoarthritis and Cartilage*, vol. 19, no. 11, pp. 1270–1285, 2011.

[11] Kenneth Maiese, "Picking a bone with wisp1 (ccn4): new strategies against degenerative joint disease," *Journal of translational science*, vol. 1, no. 3, pp. 83, 2016.

[12] Miriam G Cisternas, Louise Murphy, Jeffrey J Sacks, Daniel H Solomon, David J Pasta, and Charles G Helmick, "Alternative methods for defining osteoarthritis and the impact on estimating prevalence in a us population-based survey," *Arthritis care & research*, vol. 68, no. 5, pp. 574–580, 2016.

[13] Ariel Berger, Craig Hartrick, John Edelsberg, Alesia Sadosky, and Gerry Oster, "Direct and indirect economic costs among private-sector employees with osteoarthritis," *Journal of occupational and environmental medicine*, vol. 53, no. 11, pp. 1228–1235, 2011.

[14] Yuqing Zhang and Joanne M Jordan, "Epidemiology of osteoarthritis," *Clinics in geriatric medicine*, vol. 26, no. 3, pp. 355–369, 2010.

[15] Greg A Brown, "Aaos clinical practice guideline: treatment of osteoarthritis of the knee: evidence-based guideline," *JAAOS-Journal of the American Academy of Orthopaedic Surgeons*, vol. 21, no. 9, pp. 577–579, 2013.

[16] Bhushan R Deshpande, Jeffrey N Katz, Daniel H Solomon, Edward H Yelin, David J Hunter, Stephen P Messier, Lisa G Suter, and Elena Losina, "Number of persons with symptomatic knee osteoarthritis in the us: impact of race and ethnicity, age, sex, and obesity," *Arthritis care & research*, vol. 68, no. 12, pp. 1743–1750, 2016.

[17] Uyen-Sa DT Nguyen, Yuqing Zhang, Yanyan Zhu, Jingbo Niu, Bin Zhang, and David T Felson, "Increasing prevalence of knee pain and symptomatic knee osteoarthritis: survey and cohort data," *Annals of internal medicine*, vol. 155, no. 11, pp. 725–732, 2011.

[18] David J Hunter, Tuhina Neogi, and Marc C Hochberg, "Quality of osteoarthritis management and the need for reform in the us," *Arthritis care & research*, vol. 63, no. 1, pp. 31–38, 2011.

[19] Pradeep Suri, David C Morgenroth, and David J Hunter, "Epidemiology of osteoarthritis and associated comorbidities," *PM&R*, vol. 4, no. 5, pp. S10–S19, 2012.

[20] Elena Losina, A David Paltiel, Alexander M Weinstein, Edward Yelin, David J Hunter, Stephanie P Chen, Kristina Klara, Lisa G Suter, Daniel H Solomon, Sara A Burbine, et al., "Lifetime medical costs of knee osteoarthritis management in the united states: impact of extending indications for total knee arthroplasty," *Arthritis care & research*, vol. 67, no. 2, pp. 203–215, 2015.

[21] Mohit Bhandari, Jon Smith, Larry E Miller, and Jon E Block, "Clinical and economic burden of revision knee arthroplasty," *Clinical Medicine Insights: Arthritis and Musculoskeletal Disorders*, vol. 5, pp. CMAMD–S10859, 2012.

[22] Ilana N Ackerman, Andrew Bucknill, Richard S Page, Nigel S Broughton, Carol Roberts, Bernarda Cavka, Peter Schoch, and Caroline A Brand, "The substantial personal burden experienced by younger people with hip or knee osteoarthritis," *Osteoarthritis and cartilage*, vol. 23, no. 8, pp. 1276–1284, 2015.

[23] Linda J Sandell, "Etiology of osteoarthritis: genetics and synovial joint development," *Nature Reviews Rheumatology*, vol. 8, no. 2, pp. 77, 2012.

[24] Elena Losina, Thomas S Thornhill, Benjamin N Rome, John Wright, and Jeffrey N Katz, "The dramatic increase in total knee replacement utilization rates in the united states cannot be fully explained by growth in population size and the obesity epidemic," *The Journal of Bone and Joint Surgery. American volume.*, vol. 94, no. 3, pp. 201, 2012.

[25] Tonia L. Vincent and Fiona E. Watt, "Osteoarthritis," *Medicine*, vol. 42, no. 4, pp. 213 – 219, 2014, Rheumatology I.

[26] A.E. Nelson, "Osteoarthritis year in review 2017: clinical," *Osteoarthritis and Cartilage*, vol. 26, no. 3, pp. 319 – 325, 2018.

[27] Frank W Roemer, Michel D Crema, Siegfried Trattnig, and Ali Guermazi, "Advances in imaging of osteoarthritis and cartilage," *Radiology*, vol. 260, no. 2, pp. 332–354, 2011.

[28] Hillary J Braun and Garry E Gold, "Diagnosis of osteoarthritis: imaging," *Bone*, vol. 51, no. 2, pp. 278–288, 2012.

[29] Gwidon W Stachowiak, Marcin Wolski, Tomasz Woloszynski, and Pawel Podsiadlo, "Detection and prediction of osteoarthritis in knee and hand joints based on the x-ray image analysis," *Biosurface and Biotribology*, vol. 2, no. 4, pp. 162–172, 2016.

[30] Lior Shamir, Shari M Ling, William Scott, Marc Hochberg, Luigi Ferrucci, and Ilya G Goldberg, "Early detection of radiographic knee osteoarthritis using computer-aided analysis," *Osteoarthritis and Cartilage*, vol. 17, no. 10, pp. 1307–1312, 2009.

[31] DJ Hart, TD Spector, P Brown, P Wilson, DV Doyle, and AJ Silman, "Clinical signs of early osteoarthritis: reproducibility and relation to x ray changes in 541 women in the general population.," *Annals of the Rheumatic Diseases*, vol. 50, no. 7, pp. 467, 1991.

[32] Steven A Mazzuca, Kenneth D Brandt, and Barry P Katz, "Is conventional radiography suitable for evaluation of a disease-modifying drug in patients with knee osteoarthritis?," *Osteoarthritis and cartilage*, vol. 5, no. 4, pp. 217–226, 1997.

[33] C Peterfy, J Li, S Zaim, J Duryea, J Lynch, Y Miaux, W Yu, and HK Genant, "Comparison of fixed-flexion positioning with fluoroscopic semi-flexed positioning for quantifying radiographic joint-space width in the knee: test-retest reproducibility," *Skeletal radiology*, vol. 32, no. 3, pp. 128–132, 2003.

[34] Mark D Kohn, Adam A Sassoon, and Navin D Fernando, "Classifications in brief: Kellgren-lawrence classification of osteoarthritis," 2016.

[35] Dieuwke Schiphof, Maarten Boers, and Sita MA Bierma-Zeinstra, "Differences in descriptions of kellgren and lawrence grades of knee osteoarthritis," *Annals of the rheumatic diseases*, vol. 67, no. 7, pp. 1034–1036, 2008.

[36] David T Felson, Jingbo Niu, Ali Guermazi, Burton Sack, and Piran Aliabadi, "Defining radiographic incidence and progression of knee osteoarthritis: suggested modifications of the kellgren and lawrence scale," *Annals of the rheumatic diseases*, p. annrheumdis155119, 2011.

[37] Frank P Luyten, Matteo Denti, Giuseppe Filardo, Elizaveta Kon, and Lars Engebretsen, "Definition and classification of early osteoarthritis of the knee," *Knee Surgery, Sports Traumatology, Arthroscopy*, vol. 20, no. 3, pp. 401–406, 2012.

[38] Lior Shamir, Shari M Ling, William W Scott Jr, Angelo Bos, Nikita Orlov, Tomasz J Macura, D Mark Eckley, Luigi Ferrucci, and Ilya G Goldberg, "Knee x-ray image analysis method for automated detection of osteoarthritis," *IEEE Transactions on Biomedical Engineering*, vol. 56, no. 2, pp. 407–415, 2009.

[39] Shreyasee Amin, Michael P LaValley, Ali Guermazi, Mikayel Grigoryan, David J Hunter, Margaret Clancy, Jingbo Niu, Daniel R Gale, and David T Felson, "The relationship between cartilage loss on magnetic resonance imaging and radiographic progression in men and women with knee osteoarthritis," *Arthritis & Rheumatism*, vol. 52, no. 10, pp. 3152–3159, 2005.

[40] Thomas M Link, Robert Stahl, and Klaus Woertler, "Cartilage imaging: motivation, techniques, current and future significance," *European radiology*, vol. 17, no. 5, pp. 1135–1146, 2007.

[41] Sylvain R Duc, Christian WA Pfirrmann, Marius R Schmid, Marco Zanetti, Peter P Koch, Fabian Kalberer, and Juerg Hodler, "Articular cartilage defects detected with 3d water-excitation true fisp: prospective comparison with sequences commonly used for knee imaging," *Radiology*, vol. 245, no. 1, pp. 216–223, 2007.

[42] Felix Eckstein, Martin Hudelmaier, Wolfgang Wirth, Berthold Kiefer, Rebecca Jackson, Joseph Yu, CB Eaton, and Erika Schneider, "Double echo steady state magnetic resonance imaging of knee articular cartilage at 3 tesla: a pilot study for the osteoarthritis initiative," *Annals of the rheumatic diseases*, vol. 65, no. 4, pp. 433–441, 2006.

[43] Frank W Roemer, Ali Guermazi, John A Lynch, Charles G Peterfy, Michael C Nevitt, Nita Webb, Jing Li, Andreas Mohr, Harry K Genant, and David T Felson, "Short tau inversion recovery and proton density-weighted fat suppressed sequences for the evaluation of osteoarthritis of the knee with a 1.0 t dedicated extremity mri: development of a time-efficient sequence protocol," *European radiology*, vol. 15, no. 5, pp. 978–987, 2005.

[44] Richard Kijowski, Kirkland W Davis, Michael A Woods, Mary J Lindstrom, Arthur A De Smet, Garry E Gold, and Reed F Busse, "Knee joint: comprehensive assessment with 3d isotropic resolution fast spin-echo mr imagingdiagnostic performance compared with that of conventional mr imaging at 3.0 t," *Radiology*, vol. 252, no. 2, pp. 486–495, 2009.

[45] DG Disler, TR McCauley, CG Kelman, MD Fuchs, LM Ratner, CR Wirth, and PP Hospodar, "Fat-suppressed three-dimensional spoiled gradient-echo mr imaging of hyaline cartilage defects in the knee: comparison with standard mr imaging and arthroscopy.," *AJR. American journal of roentgenology*, vol. 167, no. 1, pp. 127–132, 1996.

[46] Charles A McKenzie, Ashley Williams, Pottumarthi V Prasad, and Deborah Burstein, "Three-dimensional delayed gadolinium-enhanced mri of cartilage (dgemric) at 1.5 t and 3.0 t," *Journal of Magnetic Resonance Imaging: An Official Journal of the International Society for Magnetic Resonance in Medicine*, vol. 24, no. 4, pp. 928–933, 2006.

[47] Ferencz J Baranyay, Yuanyuan Wang, Anita E Wluka, Dallas R English, Graham G Giles, Richard O Sullivan, and Flavia M Cicuttini, "Association of bone marrow lesions with knee structures and risk factors for bone marrow lesions in the knees of clinically healthy, community-based adults," in *Seminars in arthritis and rheumatism*. Elsevier, 2007, vol. 37, pp. 112–118.

[48] JW Landells, "The bone cysts of osteoarthritis," *The Journal of bone and joint surgery. British volume*, vol. 35, no. 4, pp. 643–649, 1953.

[49] DONALD Resnick, Gen Niwayama, and RICHARD D Coutts, "Subchondral cysts (geodes) in arthritic disorders: pathologic and radiographic appearance of the hip joint," *American Journal of Roentgenology*, vol. 128, no. 5, pp. 799–806, 1977.

[50] Stephan Reichenbach, Ali Guermazi, Jingbo Niu, Tuhina Neogi, David J Hunter, Frank W Roemer, Christine E McLennan, Gabriela Hernandez-Molina, and David T Felson, "Prevalence of bone attrition on knee radiographs and mri in a community-based cohort," *Osteoarthritis and cartilage*, vol. 16, no. 9, pp. 1005–1010, 2008.

[51] David T Felson, Sara McLaughlin, Joyce Goggins, Michael P LaValley, M Elon Gale, Saara Totterman, Wei Li, Catherine Hill, and Daniel Gale, "Bone marrow edema and its relation to progression of knee osteoarthritis," *Annals of internal medicine*, vol. 139, no. 5_Part_1, pp. 330–336, 2003.

[52] David J Hunter, Yuqing Zhang, Jingbo Niu, Joyce Goggins, Shreyasee Amin, Michael P LaValley, Ali Guermazi, Harry Genant, Daniel Gale, and David T Felson, "Increase in bone marrow lesions associated with cartilage loss: a longitudinal magnetic resonance imaging study of knee osteoarthritis," *Arthritis & Rheumatism: Official Journal of the American College of Rheumatology*, vol. 54, no. 5, pp. 1529–1535, 2006.

[53] Frank W Roemer, Ali Guermazi, M Kassim Javaid, John A Lynch, Jingbo Niu, Yuqing Zhang, David T Felson, Cora E Lewis, James Torner, and Michael C Nevitt, "Change in mri-detected subchondral bone marrow lesions is associated with cartilage loss–the most study a longitudinal multicenter study of knee osteoarthritis," *Annals of the rheumatic diseases*, 2008.

[54] Tobias Stammberger, Felix Eckstein, Karl-Hans Englmeier, and Maximilian Reiser, "Determination of 3d cartilage thickness data from mr imaging: computational

method and reproducibility in the living," *Magnetic resonance in medicine*, vol. 41, no. 3, pp. 529–536, 1999.

[55] Zohara A Cohen, Denise M Mccarthy, S Daniel Kwak, Perrine Legrand, Fabian Fogarasi, Edward J Ciaccio, and Gerard A Ateshian, "Knee cartilage topography, thickness, and contact areas from mri: in-vitro calibration and in-vivo measurements," *Osteoarthritis and cartilage*, vol. 7, no. 1, pp. 95–109, 1999.

[56] S Koo, GE Gold, and TP Andriacchi, "Considerations in measuring cartilage thickness using mri: factors influencing reproducibility and accuracy," *Osteoarthritis and cartilage*, vol. 13, no. 9, pp. 782–789, 2005.

[57] Chen Jia-xin and Liu Sen, "A medical image segmentation method based on watershed transform," in *Computer and Information Technology, 2005. CIT 2005. The Fifth International Conference on*. IEEE, 2005, pp. 634–638.

[58] CG Peterfy, A Guermazi, S Zaim, PFJ Tirman, Y Miaux, D White, M Kothari, Y Lu, K Fye, S Zhao, et al., "Whole-organ magnetic resonance imaging score (worms) of the knee in osteoarthritis," *Osteoarthritis and Cartilage*, vol. 12, no. 3, pp. 177–190, 2004.

[59] Peter R Kornaat, Ruth YT Ceulemans, Herman M Kroon, Naghmeh Riyazi, Margreet Kloppenburg, Wayne O Carter, Thasia G Woodworth, and Johan L Bloem, "Mri assessment of knee osteoarthritis: Knee osteoarthritis scoring system (koss)inter-observer and intra-observer reproducibility of a compartment-based scoring system," *Skeletal radiology*, vol. 34, no. 2, pp. 95–102, 2005.

[60] David J Hunter, Grace H Lo, D Gale, Andrew J Grainger, Ali Guermazi, and Philip G Conaghan, "The reliability of a new scoring system for knee osteoarthritis mri and the validity of bone marrow lesion assessment: Bloks (boston–leeds osteoarthritis knee score)," *Annals of the rheumatic diseases*, vol. 67, no. 2, pp. 206–211, 2008.

[61] Michael J O'Malley and Constance R Chu, "Arthroscopic optical coherence tomography in diagnosis of early arthritis," *Minimally Invasive Surgery*, vol. 2011, 2011.

[62] CW Han, CR Chu, N Adachi, A Usas, FH Fu, J Huard, and Y Pan, "Analysis of rabbit articular cartilage repair after chondrocyte implantation using optical coherence tomography," *Osteoarthritis and cartilage*, vol. 11, no. 2, pp. 111–121, 2003.

[63] Xingde Li, Scott Martin, Costas Pitris, Ravi Ghanta, Debra L Stamper, Michelle Harman, James G Fujimoto, and Mark E Brezinski, "High-resolution optical coherence tomographic imaging of osteoarthritic cartilage during open knee surgery," *Arthritis Res Ther*, vol. 7, no. 2, pp. R318, 2005.

[64] Constance R Chu, Ashley Williams, David Tolliver, C Kent Kwoh, Stephen Bruno III, and James J Irrgang, "Clinical optical coherence tomography of early articular cartilage degeneration in patients with degenerative meniscal tears," *Arthritis & Rheumatism*, vol. 62, no. 5, pp. 1412–1420, 2010.

[65] HI Keen, RJ Wakefield, and PG Conaghan, "A systematic review of ultrasonography in osteoarthritis," *Annals of the rheumatic diseases*, vol. 68, no. 5, pp. 611–619, 2009.

[66] WA Schmidt, L Volker, J Zacher, M Schlafke, M Ruhnke, and E Gromnica-Ihle, "Colour doppler ultrasonography to detect pannus in knee joint synovitis," *Clinical and experimental rheumatology*, vol. 18, no. 4, pp. 439–444, 2000.

[67] RJ Wakefield, WW Gibbon, and P Emery, "The current status of ultrasonography in rheumatology.," *Rheumatology (Oxford, England)*, vol. 38, no. 3, pp. 195–198, 1999.

[68] Frank W Roemer, Marnix Van Holsbeeck, and Harry K Genant, "Musculoskeletal ultrasound in rheumatology: a radiologic perspective," *Arthritis Care & Research*, vol. 53, no. 4, pp. 491–493, 2005.

[69] E Qvistgaard, H Kristoffersen, L Terslev, B Danneskiold-Samsøe, S Torp-Pedersen, and H Bliddal, "Guidance by ultrasound of intra-articular injections in the knee and hip joints," *Osteoarthritis and Cartilage*, vol. 9, no. 6, pp. 512–517, 2001.

[70] P Monteforte, P Sessarego, and G Rovetta, "Sonographic assessment of soft tissue alterations in osteoarthritis of the knee," *Giornale italiano di medicina del lavoro ed ergonomia*, vol. 30, no. 1, pp. 75, 2008.

[71] Giulio Coari, Annamaria Iagnocco, "Usefulness of high resolution us in the evaluation of effusion in osteoarthritic first carpometacarpal joint," *Scandinavian journal of rheumatology*, vol. 29, no. 3, pp. 170–173, 2000.

[72] Ole Mathiesen, Lars Konradsen, Søren Torp-Pedersen, and Uffe Jørgensen, "Ultrasonography and articular cartilage defects in the knee: an in vitro evaluation of the accuracy of cartilage thickness and defect size assessment," *Knee Surgery, Sports Traumatology, Arthroscopy*, vol. 12, no. 5, pp. 440–443, 2004.

[73] Esperanza Naredo, Carlos Acebes, Ingrid Möller, Fernando Canillas, Juan José de Agustín, Eugenio de Miguel, Emilio Filippucci, Annamaria Iagnocco, Carmen Moragues, Roser Tuneu, et al., "Ultrasound validity in the measurement of knee cartilage thickness," *Annals of the rheumatic diseases*, vol. 68, no. 8, pp. 1322–1327, 2009.

[74] Ali Guermazi, Felix Eckstein, Marie-Pierre Hellio Le Graverand-Gastineau, Philip G Conaghan, Deborah Burstein, Helen Keen, and Frank W Roemer, "Osteoarthritis: current role of imaging," *Medical Clinics of North America*, vol. 93, no. 1, pp. 101–126, 2009.

[75] Helen I Keen and Philip G Conaghan, "Ultrasonography in osteoarthritis," *Radiologic Clinics*, vol. 47, no. 4, pp. 581–594, 2009.

[76] Walter Grassi, Gianni Lamanna, Antonella Farina, and Claudio Cervini, "Sonographic imaging of normal and osteoarthritic cartilage," in *Seminars in arthritis and rheumatism*. Elsevier, 1999, vol. 28, pp. 398–403.

[77] M Backhaus, Th Kamradt, D Sandrock, D Loreck, J Fritz, KJ Wolf, H Raber, B Hamm, G-R Burmester, and M Bollow, "Arthritis of the finger joints: a comprehensive approach comparing conventional radiography, scintigraphy, ultrasound, and contrast-enhanced magnetic resonance imaging," *Arthritis & Rheumatism: Official Journal of the American College of Rheumatology*, vol. 42, no. 6, pp. 1232–1245, 1999.

[78] Maria Antonietta DAgostino, Philip Conaghan, Manuela Le Bars, Gabriel Baron, Walter Grassi, Emilio Martin-Mola, Richard Wakefield, Jean-Louis Brasseur, Alexander So, Marina Backhaus, et al., "Eular report on the use of ultrasonography in painful knee osteoarthritis. part 1: prevalence of inflammation in osteoarthritis," *Annals of the rheumatic diseases*, vol. 64, no. 12, pp. 1703–1709, 2005.

[79] Jonathan K Kazam, Levon N Nazarian, Theodore T Miller, Carolyn M Sofka, Laurence Parker, and Ronald S Adler, "Sonographic evaluation of femoral trochlear cartilage in patients with knee pain," *Journal of Ultrasound in Medicine*, vol. 30, no. 6, pp. 797–802, 2011.

[80] Alex M Aisen, W Joseph McCune, Anne MacGuire, Paul L Carson, Terry M Silver, S Zafar Jafri, and William Martel, "Sonographic evaluation of the cartilage of the knee.," *Radiology*, vol. 153, no. 3, pp. 781–784, 1984.

[81] Randy J Schmitz, Hsin-Min Wang, Daniel R Polprasert, Robert A Kraft, and Brian G Pietrosimone, "Evaluation of knee cartilage thickness: a comparison between ultrasound and magnetic resonance imaging methods," *The Knee*, vol. 24, no. 2, pp. 217–223, 2017.

[82] S Saarakkala, P Waris, V Waris, I Tarkiainen, E Karvanen, J Aarnio, and JM Koski, "Diagnostic performance of knee ultrasonography for detecting degenerative changes of articular cartilage," *Osteoarthritis and cartilage*, vol. 20, no. 5, pp. 376–381, 2012.

[83] MS Harkey, JT Blackburn, H Davis, L Sierra-Arévalo, D Nissman, and B Pietrosimone, "Ultrasonographic assessment of medial femoral cartilage deformation acutely following walking and running," *Osteoarthritis and cartilage*, vol. 25, no. 6, pp. 907–913, 2017.

[84] Md Belayet Hossain, Khin Wee Lai, Belinda Pingguan-Murphy, Yan Chai Hum, Maheza Irna Mohd Salim, and Yih Miin Liew, "Contrast enhancement of ultrasound imaging of the knee joint cartilage for early detection of knee osteoarthritis," *Biomedical Signal Processing and Control*, vol. 13, pp. 157–167, 2014.

[85] Amir Faisal, Siew-Cheok Ng, Siew-Li Goh, and Khin Wee Lai, "Knee cartilage segmentation and thickness computation from ultrasound images," *Medical & biological engineering & computing*, vol. 56, no. 4, pp. 657–669, 2018.

[86] Prajna Ramesh Desai and Ilker Hacihaliloglu, "Enhancement and automated segmentation of ultrasound knee cartilage for early diagnosis of knee osteoarthritis," in *Biomedical Imaging (ISBI 2018), 2018 IEEE 15th International Symposium on.* IEEE, 2018, pp. 1471–1474.

Chapter 2

Knee imaging using ultrasound, challenges

This section presents an overview of ultrasound (US) imaging of the knee, typical problems associated with US, and the importance of local phase information for processing US data.

2.1 Bone surface and cartilage appearance in ultrasound

The normal US knee image consists of uniformly distributed bone profile, monotonous echogenicity of articular cartilage, and presence of soft tissues. The articular cartilage appears as a thick band of low intensity dark pixels between the soft tissue-cartilage and cartilage-bone interfaces. Figure 2.1, shows the hypoechoic band of cartilage region surrounded by the two hyperechoic or high intensity contours on either of the side.

The healthy bone profile in 2D B-mode US image is indicated by the high intensities or bright pixels same as soft tissue interfaces. The bone surfaces appear to be blurred and has some thickness associated with it (Figure 2.1). The introduced response thickness depends on the positioning and inclination of US transducer with respect to the imaging plane [1]. The response thickness is directly associated with the inclination, that is, higher inclination produces higher response thickness.

2.2 Ultrasound imaging artifacts

US imaging is an essential part of clinical routine offering real-time imaging of patient anatomy. In the last decades advances in US transducer and system development have led to a substantial improvement of US image quality and to an ever increasing use in clinical practice. However, US signal attenuation, high level of speckle noise, limited

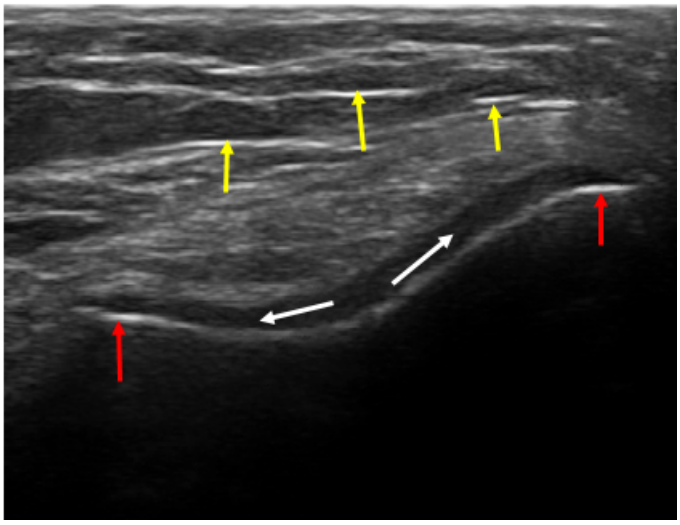

Figure 2.1: B-mode knee US image depicting cartilage region (shown with white arrows), femoral bone surface (shown with red arrows) and soft tissue interfaces (shown with yellow arrows).

FOV, and shadow artifacts are still unavoidable, and continue to challenge in the field of medical image computing. In this section, we are discussing the effect of speckle noise, shadow artifacts, and user dependency on the quality of 2D US knee image to visualize cartilage region.

2.2.1 Speckle noise

The speckle noise, also known as 'coherent interference artifact' exhibits granular appearance of various size, and intensities [2,3]. In US, the sound wave is triggered at the region of interest and the US waves that returns to the transducer is measured. The US image is formed based on the strength of received pulse. When the US wave hits the tissue or any structure that are of a size comparable to the US wavelength, then the signal undergoes scattering or reflection based on the location. Depending on the phase of the signal, the overall US signal undergoes constructive or destructive interference resulting in increase or decrease in US signal energy that are received back to the transducer. The superposition of these scattered echoes coming with random phases and amplitude interfere with each other constructively or destructively, creating high

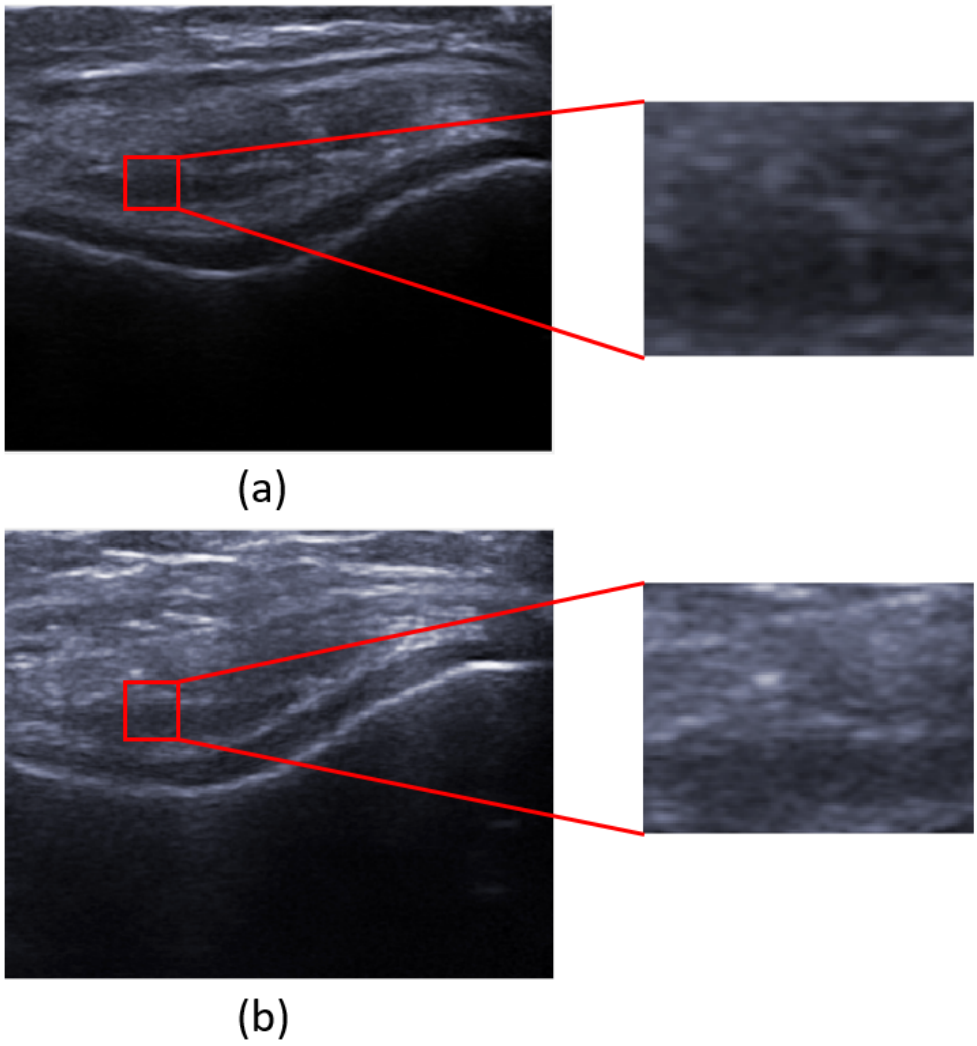

Figure 2.2: Speckle appearance in 2D US knee cartilage image for different US machine setting.

gray level of intensity of a bright(hyper echoic) and dark (hypo echoic) spots known as speckles [4]. They are more granular at low acoustic frequency than at a high frequency. The speckle noise is dependent on the phase sensitivity of a transducer, the total number of scattered beams, and their density, the distance between objects and the transducer, and the transducer acoustic frequency used to acquire the image [5]. Figure 2.2 shows the speckle noise in US knee cartilage image. The speckle noise produces poor image quality, including reduced spatial and contrast resolution . [2, 4]

Table 2.1: Speed of sound and acoustic impedance of different tissues and organs

Medium	Speed of sound c (m/s)	Impedance Z (10^6 Rayls)
Air	330	0.0004
Water	1480	1.48
Lung	600	0.18
Liver	1555	1.65
Fat	1460	1.34
Muscle	1600	1.71
Kidney	1565	1.63
Bone	4080	7.8

2.2.2 Bone shadow artifact

As discussed in section 2.2, the US image is formed from the signals returned to the transducer. The US wave propagation through any homogeneous medium is characterized by acoustic impedance Z, [6]. which describes the resistance encountered by US waves as it passes through the tissue and medium. The impedance difference between transducer and tissue can cause significant reflection of the emitted signal. When the US signal hits a high impedance structure, the amplitude of the incident signal decreases, and te echoes returning from structure beyond the high impedance structure will also deteriorates. The low intensity hypoechoic band that appears due to highly attenuation structure is called as shadowing. As shown in Table 2.1, bone has highest impedance value compared to other organ tissues. Most of the US signals are absorbed by the bone surfaces, therefore, very less energy is available for the generation of secondary reflections [7]. The associated shadow appears to be more anechoic and clean shadow [8]. Figure 2.3, shows the uniform low intensity bone shadow region beneath the high intensity bone surface.

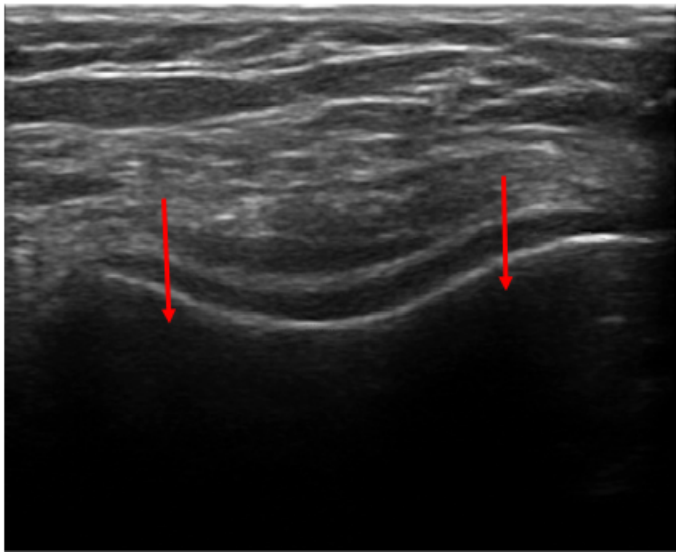

Figure 2.3: B-mode knee US image depicting shadowing (arrows) .

2.2.3 Manual data collection using hand held ultrasound transducer

The quality of acquired US image depends on the placement of transducer at specific plane to view the region of interest. The positioning and inclination angle of the transducer can introduce human error by reflecting additional cartilage thickness in the image. Figure 2.4 shows the quality of US image acquired due to proper and incorrect positioning of the transducer with respect to the imaging surface.

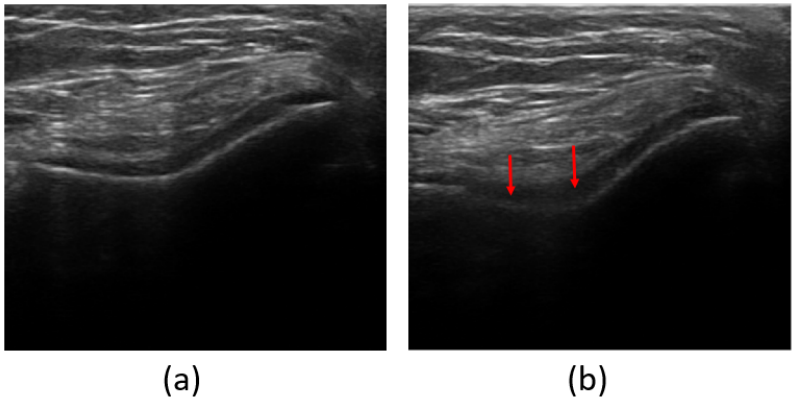

Figure 2.4: US dependency on placement and positioning of transducer by the user: (a) Correct alignment of US transducer. (b) Incorrect alignment of US transducer introducing missing bone boundary denoted by red arrows.

Due to above mentioned problems, manual segmentation and thickness measurement of cartilage region from the US images may introduce additional user dependent artifacts. The inaccurate localization of femoral surface while measuring cartilage thickness manually may add up several millimeters of additional thickness thus reporting inaccurate values.

2.3 Local phase image features

Local phase image features are crucial for analyzing the images, as they contribute to the visual appearance of the image [9]. The phase of image contains edge and detail information, which can be used to extract the features in an image. Figure 2.5, shows the qualitative analysis of importance of phase information for analyzing the image. The image is reconstructed using the phase and magnitude computed using the Fourier transform of the two images. The figure indicates that the dominant feature in the reconstructed image corresponds to the phase information of the image that was combined.

The importance of phase information for feature extraction was demonstrated by [10]. In [10], they proposed local energy model to detect the phase based features from the image. The proposed method showed that, in the image, the prominent features were found where the Fourier components were in maximal phase. Recently, there have been few studies, who successfully demonstrated the use of local phase image features to process US images for soft tissues, and to enhance the bone surface in US image for detecting the fracture. [11–18]. The local phase information is extracted by filtering the US data in frequency domain using band-pass quadrature filters [19].

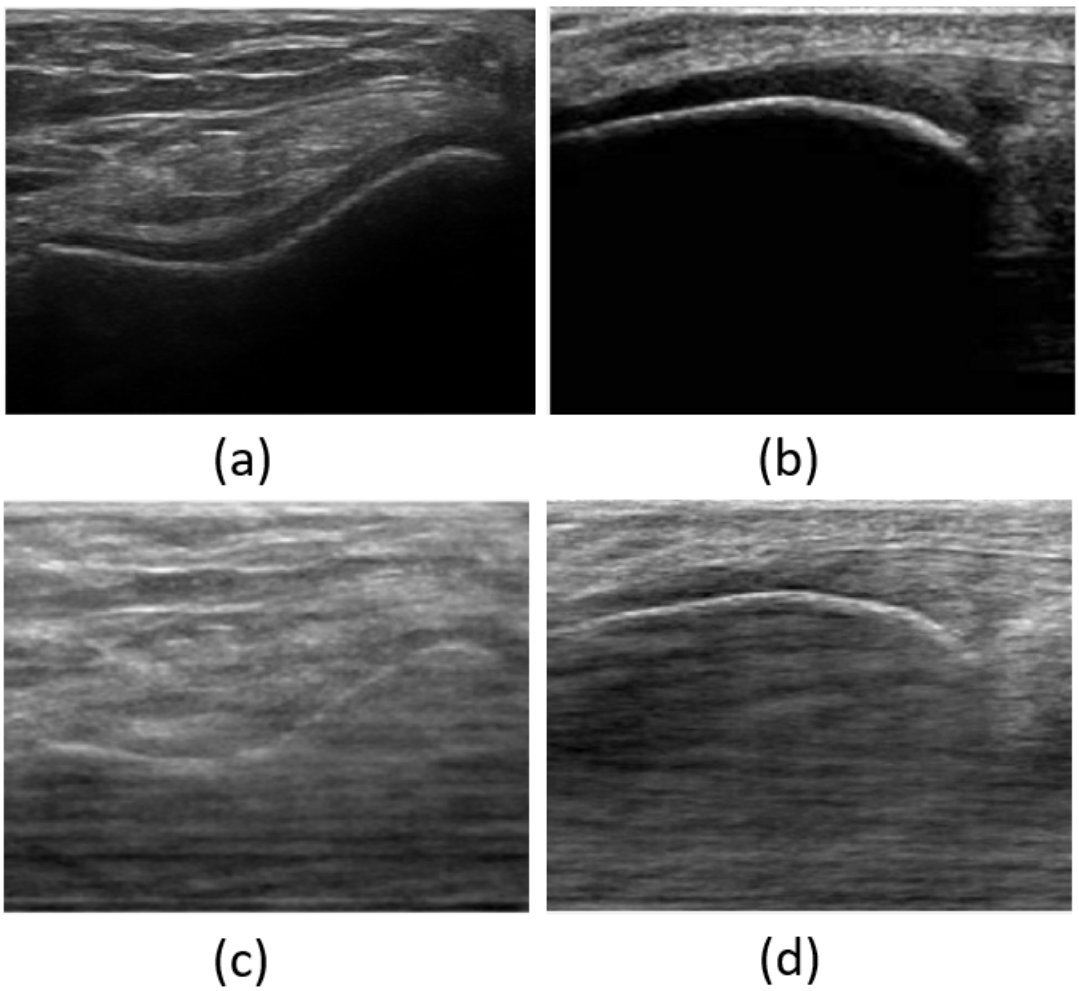

Figure 2.5: Importance of phase information. (a) B-mode US image of knee cartilage. (b) B-mode US knee cartilage image acquired by changing the US transducer position. (c) Image reconstructed by phase information from (a), and magnitude from (b). (d) Image reconstructed by phase information from (b), and magnitude from (a).

References

[1] Ilker Hacihaliloglu, "Ultrasound imaging and segmentation of bone surfaces: A review," *Technology*, vol. 5, no. 02, pp. 74–80, 2017.

[2] PNT Wells and M Halliwell, "Speckle in ultrasonic imaging," *Ultrasonics*, vol. 19, no. 5, pp. 225–229, 1981.

[3] Yael Erez, Yoav Y Schechner, and Dan Adam, "Ultrasound image denoising by spatially varying frequency compounding," in *Joint Pattern Recognition Symposium*. Springer, 2006, pp. 1–10.

[4] Oleg V Michailovich and Allen Tannenbaum, "Despeckling of medical ultrasound images," *ieee transactions on ultrasonics, ferroelectrics, and frequency control*, vol. 53, no. 1, pp. 64–78, 2006.

[5] Dan Adam, Simona Beilin-Nissan, Zvi Friedman, and Vera Behar, "The combined effect of spatial compounding and nonlinear filtering on the speckle reduction in ultrasound images," *Ultrasonics*, vol. 44, no. 2, pp. 166–181, 2006.

[6] Paul Suetens, *Fundamentals of medical imaging*, Cambridge university press, 2002.

[7] Myra K Feldman, Sanjeev Katyal, and Margaret S Blackwood, "Us artifacts," *Radiographics*, vol. 29, no. 4, pp. 1179–1189, 2009.

[8] Ammar Hindi, Cynthia Peterson, and Richard G Barr, "Artifacts in diagnostic ultrasound," *Reports in Medical Imaging*, vol. 6, pp. 29–48, 2013.

[9] JS Lim, "The importance of phase in signals," *Proc. IEEE*, vol. 69, pp. 529–41, 1981.

[10] M Concetta Morrone and Robyn A Owens, "Feature detection from local energy," *Pattern recognition letters*, vol. 6, no. 5, pp. 303–313, 1987.

[11] Matthew Mellor and Michael Brady, "Phase mutual information as a similarity measure for registration," *Medical image analysis*, vol. 9, no. 4, pp. 330–343, 2005.

[12] Vicente Grau and J Alison Noble, "Adaptive multiscale ultrasound compounding using phase information," in *International Conference on Medical Image Computing and Computer-Assisted Intervention*. Springer, 2005, pp. 589–596.

[13] Djamal Boukerroui, J Alison Noble, Marc C Robini, and Michael Brady, "Enhancement of contrast regions in suboptimal ultrasound images with application to echocardiography," *Ultrasound in medicine & biology*, vol. 27, no. 12, pp. 1583–1594, 2001.

[14] Miguel Mulet-Parada and J Alison Noble, "2d+ t acoustic boundary detection in echocardiography," *Medical image analysis*, vol. 4, no. 1, pp. 21–30, 2000.

[15] Ilker Hacihaliloglu, Rafeef Abugharbieh, Antony J Hodgson, and Robert N Rohling, "Bone surface localization in ultrasound using image phase-based features," *Ultrasound in medicine & biology*, vol. 35, no. 9, pp. 1475–1487, 2009.

[16] Ilker Hacihaliloglu, Rafeef Abugharbieh, Antony Hodgson, and Robert Rohling, "Bone segmentation and fracture detection in ultrasound using 3d local phase features," in *International Conference on Medical Image Computing and Computer-Assisted Intervention*. Springer, 2008, pp. 287–295.

[17] Ilker Hacihaliloglu, Rafeef Abugharbieh, Antony J Hodgson, Robert N Rohling, and Pierre Guy, "Automatic bone localization and fracture detection from volumetric ultrasound images using 3-d local phase features," *Ultrasound in medicine & biology*, vol. 38, no. 1, pp. 128–144, 2012.

[18] Ilker Hacihaliloglu, Abtin Rasoulian, Robert N Rohling, and Purang Abolmaesumi, "Local phase tensor features for 3-d ultrasound to statistical shape+ pose spine model registration," *IEEE transactions on Medical Imaging*, vol. 33, no. 11, pp. 2167–2179, 2014.

[19] Djamal Boukerroui, J Alison Noble, and Michael Brady, "On the choice of band-pass quadrature filters," *Journal of Mathematical Imaging and Vision*, vol. 21, no. 1-2, pp. 53–80, 2004.

Chapter 3

Methods

This chapter presents the enhancement and region based segmentation algorithms proposed to address the limitation in assessing the knee cartilage from US images. The definitions of qualitative and quantitative metrics is explained further in this chapter.

The proposed framework consists of four main sub processes: cartilage image enhancement, femoral bone extraction for automated seed initialization, cartilage segmentation using region based algorithms and mean thickness computation. The seed initialization process is shown in dotted box which includes localization and extraction of bone surface using local phase image filtering (Figure 3.1).

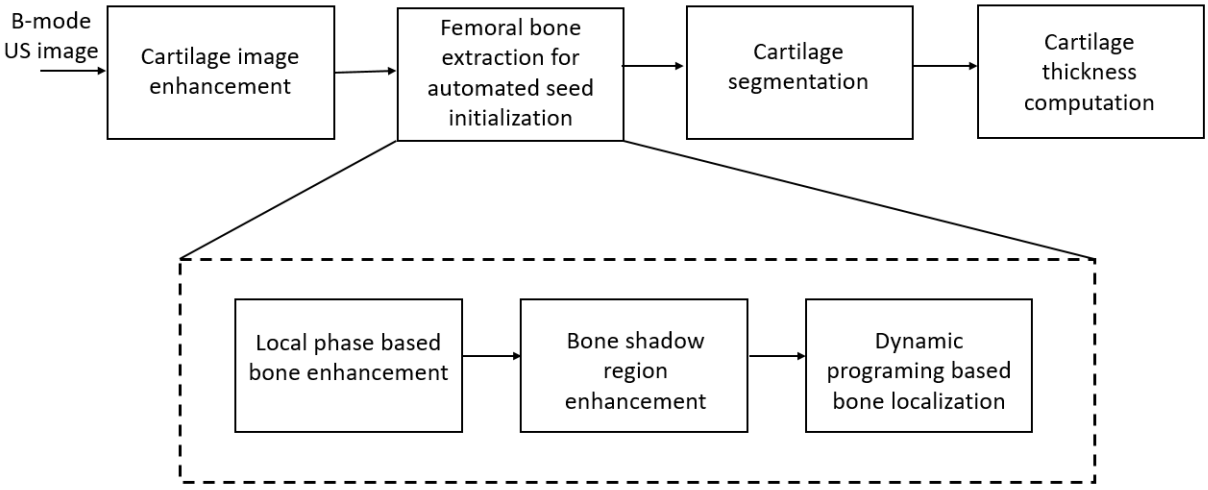

Figure 3.1: Flowchart of the proposed method

3.1 Cartilage image enhancement

The main objective of image enhancement is to enhance the given input image so that the output of the enhancement is suitable to the specific application. Enhancement of the image takes place in contrast, edges, and boundaries based on the required output. Enhancement will not increase the original information content of the data instead, it will increase the dynamic range of specific features as chosen.

The traditional approaches to enhance 2D US image based on intensity variant methods such as thresholding, gradient based methods have shown significant limitations due to non-uniform intensity across the images [1–3]. In US image, the soft tissue, and bone surfaces are denoted as high intensity values, therefore, using intensity variant methods would enhance the soft tissue interface as well, which could hinder the segmentation of bone-cartilage region. The use of local phase features allows the enhancement of bone surfaces in the image irrespective of intensity variations and contribute towards the appearance of the image. As discussed in section 2.3, the image phase information is an important consideration for the interpretation of visual appearance or features in an image. For local phase filtering, the Log-Gabor filters are used as they offer orientation selectivity [4].

The Log-Gabor filter is a symmetry based filter which indicates even and odd response of Fourier transform (FT). In 2D US images, the bone surface appears to be blurred with non-uniform intensity throughout the bone surface. The US shows ridge like edges at the bone boundaries, therefore, we look for ridge like features to enhance the bone regions for enhancing the 2D US images. The 2D Log-Gabor filter function is defined as [5],

$$G(\omega, \phi) = exp[-\frac{(log(\omega/\omega_0))^2}{2(log(k/\omega_0))^2} + \frac{(\phi - \phi_0)^2}{2\sigma_\phi}] \tag{3.1}$$

Here, $\sigma_\phi = \Delta\phi/s$ evaluates the angular bandwidth $\Delta\Omega$ as, $\Delta\Omega = 2 \times \sigma_\phi\sqrt{2 \times log2}$. $\Delta\phi$ denotes the angular separation between neighboring orientation. In 2D Log-Gabor filter, the radial component controls the frequency of band of the filter response and the angular component controls the orientation of the filter response. When the orientation

of the Log-Gabor filter is in phase with orientation of bone surface, it allows for the enhancement of bone features from the US images while suppressing the other soft tissue interfaces and US artifacts.

Let $I(x)$ be the signal to be analyzed and $M_s^e(x) = real(F^{-1}(G(\omega)))$ and $M_s^o(x) = imag(G(\omega))$ denoting even and odd response of Log-Gabor filters then, the local amplitude $A_s(x)$ and local phase $\phi_s(x)$ at given filter scale s is computed as,

$$\begin{aligned} e_s(x) = I(x) * M_s^e(x); \;\; o_s(x) = M_s^o(x) \\ A_s(x) = \sqrt{e_s(x)^2 + o_s(x)^2}; \;\; \phi_s(x) = arctan(o_s(x)/e_s(x)) \end{aligned} \tag{3.2}$$

Based on equation 3.2, the local phase information for 2D image is will result in the response of the even filters ($e_{rs}(x, y)$) and odd filter ($o_{rs}(x, y)$), local phase based image feature descriptor is constructed as the difference of these responses over a number of scales as, [6]

$$USE(x, y) = \frac{\sum_r \sum_s [[e_{rs}(x, y) - o_{rs}(x, y)] - T_r]}{\sum_r \sum_s \sqrt{e_{rs}^2(x, y) - o_{rs}^2(x, y)} + \epsilon}. \tag{3.3}$$

Where, $e(x, y)$ and $o(x, y)$ represents the Log-Gabor even and odd symmetry filter response on input B-mode US image US(x,y). The r and s represents the filter orientation and the scale, ϵ is a constant used to avoid division by zero and T_r is a noise dependent threshold calculated as a specific number κ of standard deviation (σ) and the mean (μ) of the local energy distribution due to noise as, $T = \mu + \kappa\sigma$.

Since the enhancement is based on the local phased based feature, it is independent of US machine settings. Figure 3.2 shows the enhanced $USE(x, y)$ image, where the bone-cartilage region is enhanced compared to the original B-mode US image. The enhanced image is used as an input to automated bone surface segmentation which is explained in next section.

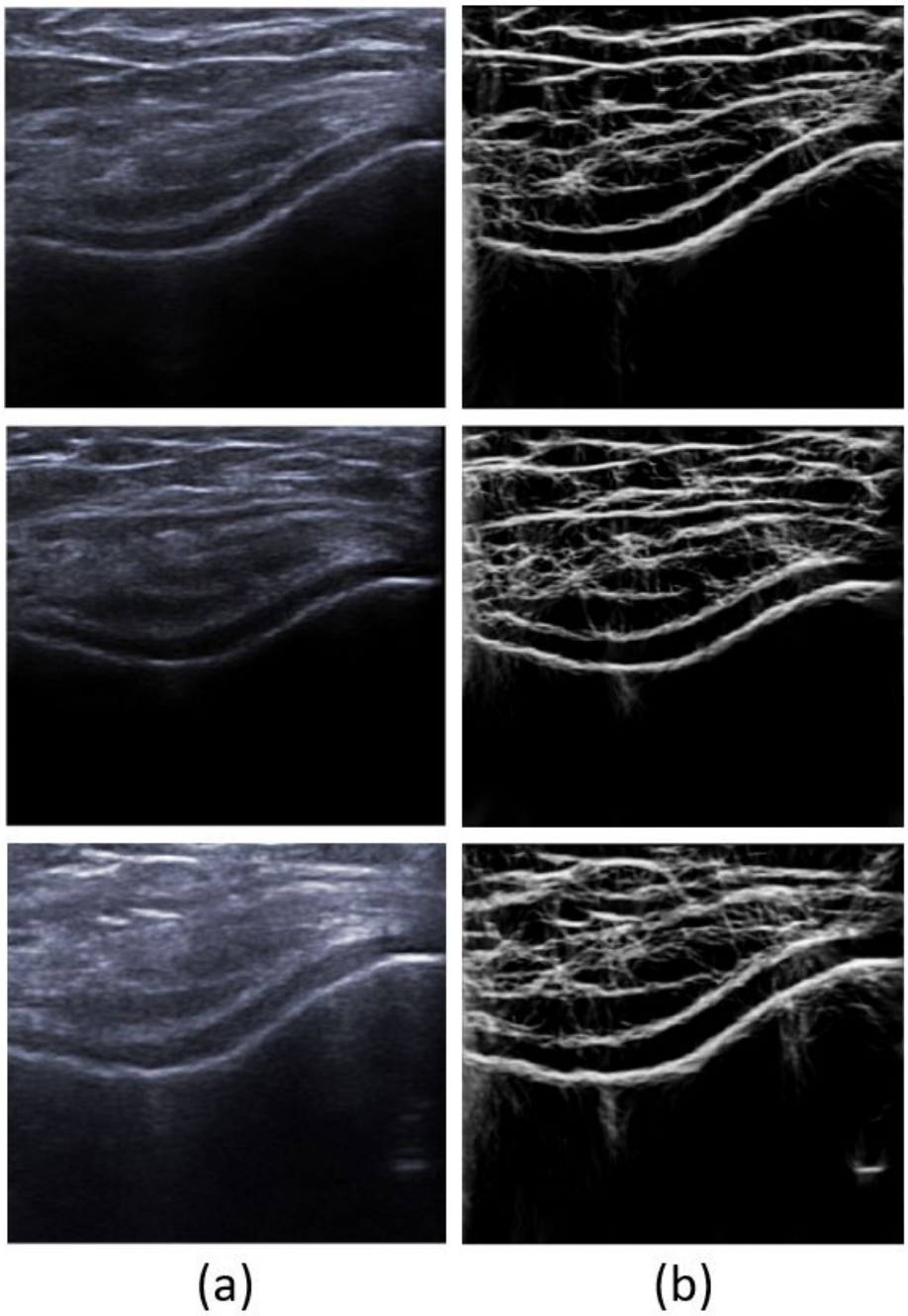

Figure 3.2: In vivo US image enhancement: Column (a) In vivo B-mode US image $US(x, y)$. Column (b) Enhanced US image $USE(x, y)$.

3.2 Automated seed initialization

The selection of initial seed points are crucial step for image segmentation, as the overall performance of the algorithm is dependent on the initial seeds. The seeds can be selected

either manually or automatically. But for effective and accurate analysis of an image, the process should involve least human interactions. While selecting the initial seed points, we should note that, the selected seed pixels must be similar to its neighboring pixels to allow for region growing, at least one seed pixel should be generated for every region in the image, and seeds of different neighboring regions should not be connected to each other [7]. In the proposed framework, automatically extracted femoral bone surface is used as the initial seed for the region based segmentation algorithm. This section presents the automated extraction of bone surface using local phase features, and signal transmission maps.

3.2.1 Bone feature enhancement

As mentioned in earlier section, US scan profile is correlated with the orientation of the transducer and appears ridge like edges along the scan lines. To localize and extract the bone surface they are further enhanced using three different local phase features specifically local phase tensor($LPT(x,y)$), local weighted mean phase angle ($LwPA(x,y)$) and local phase energy ($LPE(x,y)$).

The $LPT(x,y)$ is computed using gradient energy tensor (GET) for simultaneous analysis of local phase and orientation [8]. The GET filter response is defined as,

$$GET(US_{DB}(x,y)) = T_{even} + T_{odd} = \begin{bmatrix} GET_{11} & GET_{12} \\ GET_{21} & GET_{22} \end{bmatrix} \tag{3.4}$$

In the above equation, T_{even} and T_{odd} represents the symmetric and asymmetric filter responses Which are calculated as,

$$T_{even} = [H(US_{DB}(x,y))][H(US_{DB}(x,y))]^T, \tag{3.5}$$

$$T_{odd} = -0.5 \times ([\nabla US_{DB}(x,y)][\nabla\nabla^2 US_{DB}(x,y)]^T + [\nabla\nabla^2 US_{DB}(x,y)]\nabla US_{DB}(x,y)]^T). \tag{3.6}$$

Here the H, ∇ and ∇^2 denotes the Hessian, Gradient and Laplacian operations. $US_{DB}(x,y)$ is a distance weighted band-pass filtered US image which allows masking of soft tissue

interfaces that are closer to the transducer surface and allows to visualize the bone surfaces that are located deeper in the image. Using even and odd symmetry responses of Log-Gabor filter, The $LPT(x, y)$ is determined as,

$$LPT(x, y) = \sqrt{T_{even}^2 + T_{odd}^2} \times cos(\phi) \tag{3.7}$$

In the above equation, ϕ represents the instantaneous phase obtained from the filter responses [9].

The $LPE(x, y)$ and $LwPA(x, y)$ are computed to provide more bone surface representation with less soft tissue interface. These two local features are calculated using monogenic signal ($US_M(x, y)$) [10], which is determined using Riesz filter, whose Fourier domain representation is given as,

$$H_1(u_1, u_2) = \frac{u_1}{\sqrt{u_1^2 + u_2^2}} \quad H_2(u_1, u_2) = \frac{u_2}{\sqrt{u_1^2 + u_2^2}} \tag{3.8}$$

The $US_M(x, y)$ is formed by using band pass filtered $LPT(x, y)$ and Riesz component as,

$$US_M(x, y) = [LPT_B(x, y), LPT_B(x, y) \times h_1(x, y), LPT_B(x, y) \times h_2(x, y)]. \tag{3.9}$$

Here, $h_1(x, y)$ and $h_2(x, y)$ represents the spatial domain response of Riesz filter. The α-scale space derivative quadrature filters (ASSD) is used for band pass filtering of $LPT(x, y)$, as they have shown better edge detection on US images. The ASSD filter component is defined as [11]:

$$ASSD(\omega) = \begin{cases} n_c \omega^a exp(-(\sigma\omega)^{2\alpha}) & \omega \geq 0 \\ 0 & otherwise \end{cases} \tag{3.10}$$

where, a represents the derivative parameter which is chosen to be $a > 1$ to satisfy the DC condition. n_c is the normalization constant and σ is the filter α-scale parameter.

The $LPE(x, y)$ and $LwPA(x, y)$ are constructed as,

$$LPE(x,y) = \sum_{sc} |US_{M1}(x,y)| - \sqrt{US^2_{M2}(x,y) + US^3_{M2}(x,y)} \tag{3.11}$$

$$LwPA(x,y) = \arctan \frac{\sum_{sc} US_{M1}(x,y)}{\sqrt{\sum_{sc} US^2_{M1} + \sum_{sc} US^2_{M2}(x,y)}} \tag{3.12}$$

Where, sc represents the number of scales. The $LPE(x,y)$ denotes the underlying shape of bone boundary and $LwPA(x,y)$ preserves all structural details of US image. The final local phase bone image ($LP(x,y)$) is obtained by combining all the three phase features as, $LP(x,y) = LPT(x,y) \times LPE(x,y) \times LwPA(x,y)$. The combination of the three phase feature images results in the suppression of soft tissue interfaces while keeping the bone surfaces more compact and localized (Figure 3.3). The enhanced image $LP(x,y)$ image is used for enhancement and extraction of bone shadow regions.

3.2.2 Bone shadow enhancement

The bone shadow region enhancement is based on confidence map (CM) approach using $LP(x,y)$ image [9]. The framework, is modeled using US signal scattering and attenuation information which are combined as,

$$CM_{LP}(x,y) = US_A(x,y)BSE(x,y) + (1 - US_A(x,y))\rho. \tag{3.13}$$

Here $CM_{LP}(x,y)$ represents the CM image using [12], $US_A(x,y)$ is US signal transmission map, ρ is an echogenicity constant of surrounding tissue and $BSE(x,y)$ is enhanced bone shadow image. The $US_A(x,y)$ is minimized using below function as,

$$\frac{\lambda}{2}||US_A(x,y) - CM_{LP}(x,y)||^2_2 + \sum_{j \in x} ||W_j o(D_j * US_A(x,y))||_1 \tag{3.14}$$

Here, o represents element-wise multiplication, x is an index set and $*$ is convolution operator. W_j is a weighting matrix calculated as $W_j(x,y) = exp(-|D_j(x,y) * CM_{LP}(x,y)|^2)$. D_j is computed using higher order differential filters which enhances bone features in local regions while suppressing image noise. The $BSE(x,y)$ is computed using $US_A(x,y)$ as,

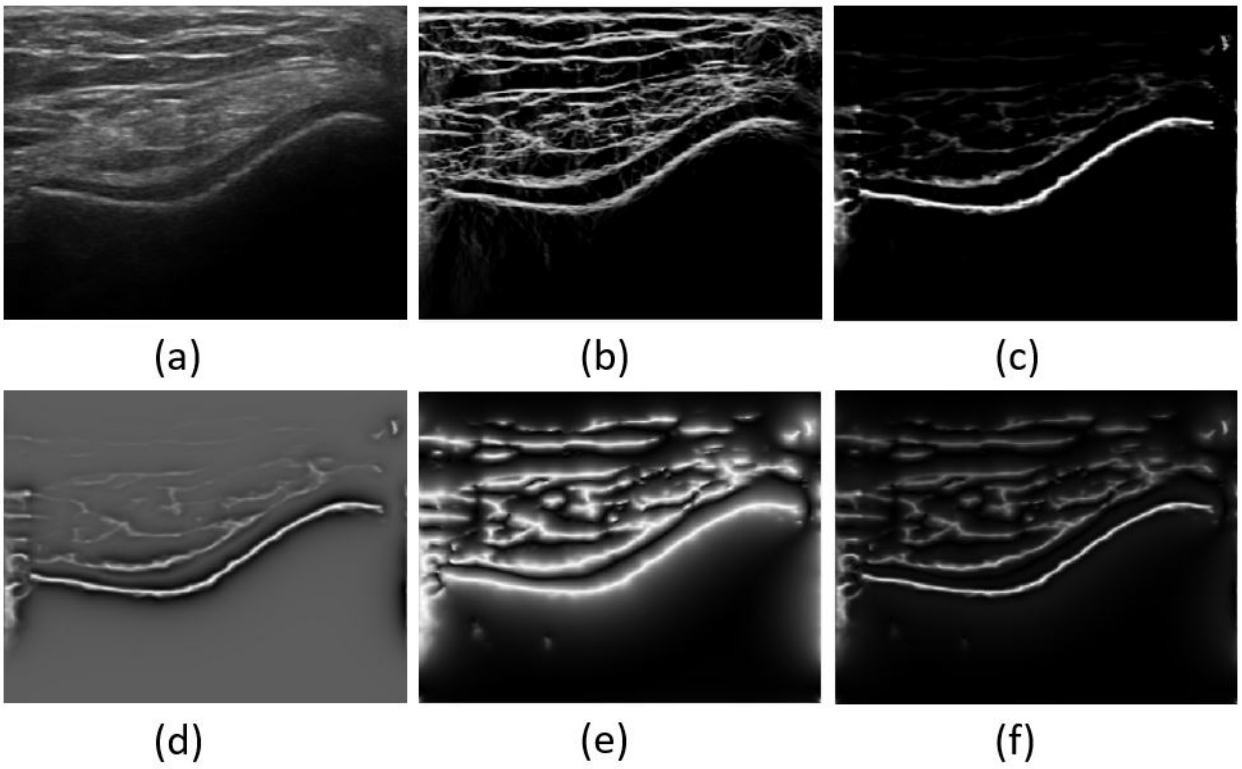

Figure 3.3: Local phase based bone surface enhancement. (a) Input original B-mode US image $US(x, y)$. (b) Enhanced US image $USE(x, y)$. (c) Local phase tensor $LPT(x, y)$ image. (d) Local phase energy $LPE(x, y)$ image. (e) Local weighted mean phase angle $LwPA(x, y)$ image. (f) Local phase $LP(x, y)$ image.

$$BSE(x, y) = [(CM_{LP}(x, y) - \rho)/[max(US_A(x, y), \epsilon)]^{\delta}] + \rho \tag{3.15}$$

Here δ is tissue attenuation coefficient, and ϵ is a constant used to avoid the divide by zero. The $BSE(x, y)$ and $LP(x, y)$ images are used during the bone surface segmentation method which is explained in the next section.

3.2.3 Bone surface extraction

The bone surface is segmented by assuming that for each scan line in US image, we have only one pixel that belongs to the bone surface [6]. The bone localization denoted as, $BL(s)$ is obtained by minimizing the cost function that is composed of internal energy($E_{int}(x,y)$) and external energy ($E_{ext}(x,y)$). The $E_{int}(x,y)$ is determined by masking $LP(x,y)$ image with $BSE(x,y)$ which provides the probability map and $E_{ext}(x,y)$ is achieved by dividing the US image into three regions marked as bone region, bone less region and the region between the two i.e., jump region which are defined as,

$$E_{ext}(i,j) = \begin{cases} \nu||\frac{dBL}{ds}||^2 + \xi||\frac{d^2BL}{ds^2}||^2 + \varsigma & Bone\,region \\ JumpCost & Jump\,region \\ \nu D_1^2 + \xi D_2^2 & Boneless\,region \end{cases} \tag{3.16}$$

Here, ν and ξ are weights of smoothness and curvature and ς is a negative scalar to ensure the bone connectivity. $BL(s)$ is minimized using local-phase based image guided dynamic programming as,

$$BLmin(i,j) = E_{int}(i,j) + min_k[BLmin(k,j-1) + E_{ext}(k,j)], \tag{3.17}$$

Here, $BLmin(i,j)$ denotes the minimum cost function moving from first column to the pixel in the i^{th} row and j^{th} column and the k represents the row index of the image. Figure 3.4 shows enhanced bone shadow image, where the overlying soft tissues above the bone surface is represented with uniform intensity, and the shadow region is represented with low intensity depicting low probability value that the signal reaching back to the transducer imaging array. The $BSE(x,y)$ shows clear transition from soft tissue interface to bone surface by depicting a sharp intensity change between two interfaces.

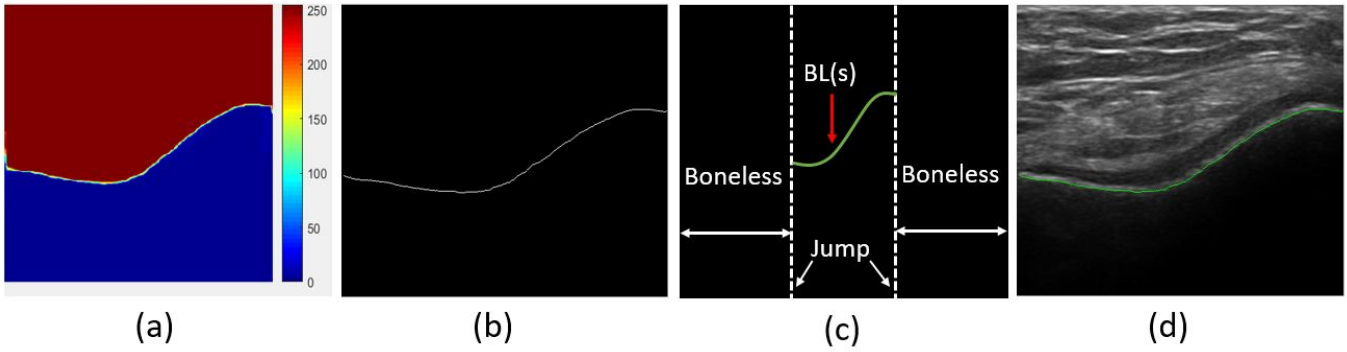

Figure 3.4: Bone surface segmentation (a) Enhanced bone shadow image BSE(x,y) (low intensity is denoted with blue, and high intensity is denoted with dark red color coding). (b) Bone probability image. (c) Regions showing bone, boneless, and jump. (d) Segmented bone surface overlaid on original B-mode US image

3.3 Cartilage segmentation

The main objective of image segmentation is to gather information for an easy analysis of features in the image. A good segmentation will provide early disease diagnosis and better clinical planning. There are several image segmentation techniques such as threshold, boundary based, region based and hybrid techniques and among them region based technique is widely used for the improved convergence and robustness [13]. The region based technique uses homogeneity property of the region i.e., all the neighboring pixels within one region have similar value or belongs to a specific region. The overall idea is to split an image into region of maximum homogeneity [14–17]. The selection of homogeneity criteria is important for segmentation performance. The user imposes hard constraints for segmentation by defining pixels as seeds that form the part of the region of interest (object) and background.

In this work, the cartilage segmentation is evaluated using RW, watershed and graph-cut methods for as they have shown better performance with prior shape knowledge. Watershed is widely used in medical image segmentation because of its ease of use, lower computing time and complete division of image with low contrast and weak boundaries. The segmented results provide closed contours thus eliminating

the post processing such as contour joining [18–22]. RW segmentation is advantageous over non-smoothness of the boundaries(metrication error), preference for shorter boundaries(shrinking bias), boundary length regularization and number of initial seeds [17, 23–25]. The graph-cuts are gaining its importance in image segmentation due to its good accuracy and performance [26–28].

3.3.1 Random walker image segmentation

In RW, the input image is represented as the graph $G = (V, E)$ where V corresponds to pixels and E are the edges connecting each pair of adjacent pixels [23]. The edges are weighted based on the pixel intensities and gradient values such that the edge with the highest gradient value is weighted more. The weighted function w_{ij} is given as,

$$w_{ij} = exp(-\beta(g_i - g_j)^2), \forall_{(i,j)} = 1, N; ij \tag{3.18}$$

Where g_i and g_j are the pixel intensities at each pixel v_i and v_j, and β is a constant. The user labels pixels as foreground and background then each unlabeled pixel release a random walk, which is classified based on the probability values of each unlabeled pixel reaching to the labeled pixel. The probability for each unlabeled pixel $x_U$is calculated as,

$$(L_U + \gamma I_U)x_U = -B^T x_s + \gamma\lambda \tag{3.19}$$

Where L represents the Laplacian of the graph, I is the identity matrix a, x is the probability vector of each pixel, λ is an optional vector of prior probabilities weighted by γ and U, S denotes unlabeled and labeled seeds.

3.3.2 Watershed image segmentation

In watershed algorithm, the gray image is transformed as a topographic relief. The objective of watershed transform is to find the 'catchment basins' and 'watershed ridge lines' which divides the neighboring catchment basin in the image [21]. In traditional watershed algorithm, a hole is punched in each local minima of the relief and the entire topography is flooded from below of the relief by letting the water through the hole rising at the uniform rate. When the rising water in catchment basin is about to merge,

a dam is built around the basin to stop the merging. These dam boundaries corresponds to the divide lines of watershed.

A marker controlled watershed algorithm is an enhancement of the traditional watershed algorithm which defines a marker and a segmentation function for efficient segmentation of objects with boundaries expressed as ridges. The markers are placed as an internal (foreground) associated with the region of interest and external marker (background) associated with the backgrounds. In traditional watershed, the catchment basin of image function f is defined as $X_{h_{max}}$ obtained after the recursion of following function,

$$\begin{aligned} X_{h_{min}} &= T_{h_{min}}(f) \\ X_{h+1} &= MIN_{h+1} \cup IZ_{T_{h+1}(f)}(X_h), \;\; h_{min} \leq h < h_{max} \end{aligned} \tag{3.20}$$

Where T_h is the threshold, MIN_h is the union of all regional minima. In marker based watershed, we impose minima to the image function f at specific locations denoted as Markers (M). The new image function g is defined as,

$$g(p) = \begin{cases} h_{min-1} \;\; if \; p \in M \\ f(p) \;\; otherwise \end{cases} \tag{3.21}$$

Here p represents the pixel coordinates and h_{min-1} represents a new value dedicated for initial markers and the new recursion function is given as,

$$\begin{aligned} X_{h_{min-1}} &= T_{h_{min-1}}(g) \\ X_{h+1} &= IZ_{T_{h+1}(g)}(X_h), \;\; h_{min-1} \leq h < h_{max} \end{aligned} \tag{3.22}$$

3.3.3 Graph-cut image segmentation

The graph-cut segmentation algorithm [26] is similar to the RW, where the input 2D image is represented as an undirected graph $G = (V, E)$, which is defined as the set of nodes and set of undirected edges (E), where each pair of the connected node is represented by a single edge $e = p, q \in E$ The graph consists of two special terminal nodes S(source) and T(sink) that represents the foreground and background labels. Each edge $e \in E$ is assigned a non-negative weight w_e. The cut divides the nodes between the terminals where, $s - t$ is a subset of edges $C \in E$ such that the terminal S

and T get separated as, $G = (V, E/C)$. The cost of cut is given as the sum of weights on edges , which is represented as

$$|C| = \sum_{e \in C} w_e \tag{3.23}$$

3.3.4 Seed initialization

The ideal seed points for region based segmentation methods must lie inside the region, and should be near the center of the region of interest. The distance from the foreground seed pixel to its neighboring pixels should be small enough to allow continuous growing. The automatically extracted bone surfaces are used as initial seeds for the cartilage segmentation algorithm. For the RW segmentation algorithm, the background seeds were initialized by translating the automated segmented bone surfaces 4.7 mm towards the bone shadow region and 4.7 mm towards the soft tissue region above the cartilage. Foreground regions were initialized by translating the bone surface 1.1 mm towards the US transducer inside the cartilage region. For watershed algorithm, the internal markers were initialized with the translation of 1.4 mm and the external marker were initialized on the localized bone surface and with the translation of 5.5 mm above the cartilage region. For the graph-cut algorithm, the foreground seeds were marked by translating the bone surface by 1.18 mm and background seeds with the translation of 4.4 mm above and below the cartilage region. Figure 3.5 shows the initial seed placement for the segmentation algorithm.

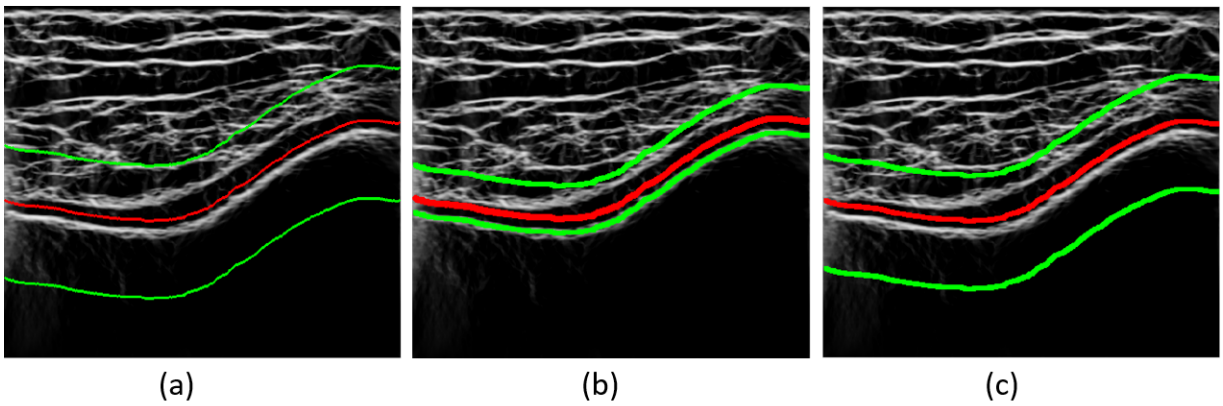

Figure 3.5: Seed Initialization on enhanced US image (Red: Foreground seeds, Green: background seeds): (a) Foreground and background seeds RW segmentation algorithm. (b) Internal and external markers for watershed algorithm. (c) Foreground and background seeds for graph-cut algorithm.

3.4 Cartilage thickness measurement

Accurate and precise measurement of cartilage thickness is an important tool for development of new methods for earlier diagnosis of OA. Traditionally, the cartilage thickness is measured manually by drawing a line between the cartilage region and synovial space. Various approaches have been proposed for automatic measurement of cartilage thickness from MRI knee scans [29–36]. In [29], the thickness is defined using Euclidean distance between bone cartilage interface and cartilage-synovium interface. In another approach, Laplace's equation is used where the top and bottom surfaces are set to fixed potentials. The Laplace equation is solved for cartilage volume to obtain a scalar field that divides the cartilage into sub-layers. The cartilage thickness is defined by length of streamlines that connect points on inter and outer interfaces of the cartilage. In [31], the thickness is computed using deformable models. Here the thickness is evaluated at every node of the surface mesh of the cartilage. Here, [33] the thickness was measured using proximity method to compute the shortest distance from each point on a given surface to the closest point on the opposing surface. The most common approach is defining the thickness as the distance between two points where the normal vector in a central axis intersects the upper and lower surfaces [35]. This method determines

the thickness distribution throughout the surface independent of section location and orientation. In normal vector method, each cartilage plate is defined as different object, surface-to-surface measurements are generated by forcing the normal vectors of opposite sides to be almost anti-parallel to each other. This leads to the artifacts to edges of cartilage plates.

In this framework, the cartilage thickness was computed using Euclidean distance map from the segmented image. The distance values corresponding to the automatically extracted cartilage boundary are averaged for the final thickness calculation. This analysis was repeated for the manually segmented and all automatically segmented cartilage regions during quantitative validation. Figure 3.6 shows example distance map image, and the extracted cartilage boundary used during thickness calculation.

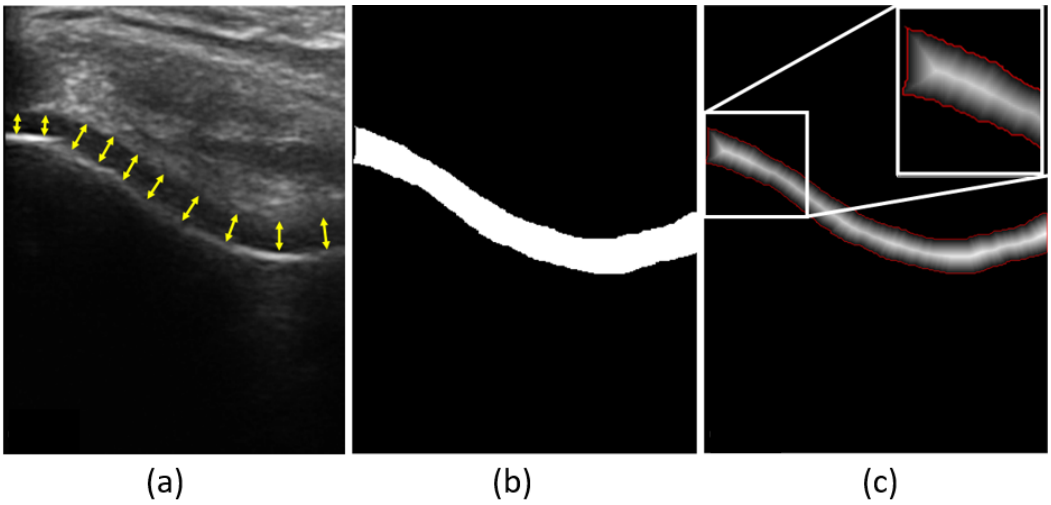

Figure 3.6: Cartilage thickness measurement: (a) Manual thickness measurement using ten anatomical landmarks shown with yellow arrows. (b) Automatically segmented cartilage. (c) Distance map obtained from the segmented image shown in (b), Red pixels denote the cartilage boundary.

The distance is computed at each pixel from the segmented results and the average cartilage thickness is reported. Measured thickness were compared to manually measured thickness using Bland-Altman plots.

3.5 Data Acquisition

The written consent was obtained prior to US scan for total 200 2D images from 10 healthy volunteers. The scans were acquired using 14-5 MHz linear US transducer with a depth setting of 3.5 cm. During the scan, the knee was positioned at 90° of flexion, and US transducer was placed transversely in line with the medial and femoral condyle above the superior edge of the patella (Figure 3.7). Different scans of cartilage were obtained from both left and right knee joints. The results of the proposed framework were validated using dice similarity coefficient (DSC) against the manually segmented image by an expert. The proposed method was implemented in MATLAB R2017a software package and run on a 3.40 GHz Intel CoreTM i7-4770 CPU, 16 GB RAM windows PC. For bone shadow enhancement, λ=2 and tissue echogenicity constant ρ was chosen as 90% of the maximum intensity value of $CM_{LP}(x, y)$. η=2, β=90 and γ=0.03 were set as constant to obtain $CM(x, y)$ and $CM_{LP}(x, y)$. For bone localization, ν=50, ξ=100, ς=0.15, $Jumpcost$=0.8, $D_1 = D_2$ =1 were set as constant values.

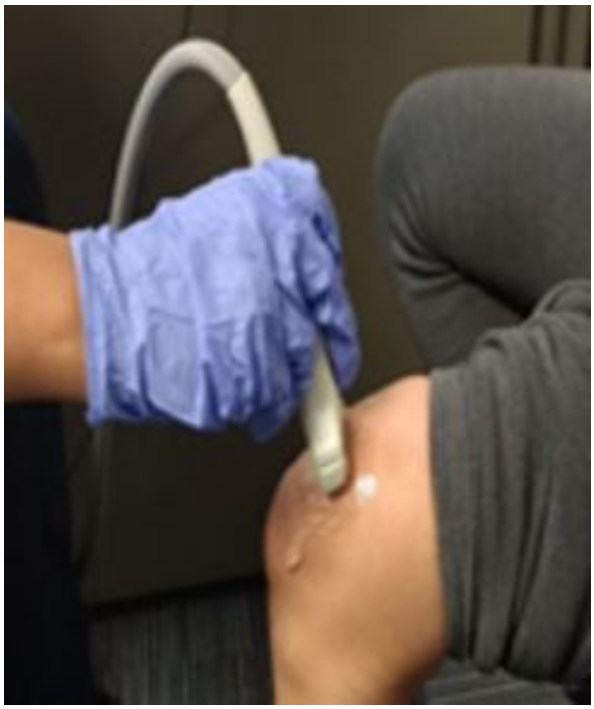

Figure 3.7: Participant setup and US probe positioning.

3.6 Quantitative analysis

The quality of segmentation results can be interpreted using quantitative measurements to validate its accuracy and reproducibility. The quantitative evaluation is done to evaluate following segmentation effects [38].

Under segmentation: Two or more regions of the foreground object is represented by a single region in the segmentation result.

Over segmentation: A region of the interest or foreground object is represented by two or more regions in the segmentation result.

The quantitative measurement of automated segmented results with ground truth segmentation data that were manually generated are evaluated using 2×2 decision matrix [39]. The decision matrix defines the term true positive (TP), true negative (TN), false positive (FP) and false negative (FP). Table 3.1 refers to the definition of decision matrix terms.

Table 3.1: Summary of decision matrix terms and their definitions

Value	Definition
TP	Pixels correctly detected as foreground
FP	Pixels falsely detected as foreground
TN	Pixels correctly detected as background
FN	Pixels falsely detected as background

Recall and precision are two important measures to validate segmentation algorithms as they are sensitive to under and over segmentation [38]. Recall indicates the proportion of boundary pixels in the ground truth that are successfully detected by the segmentation algorithm. Whereas precision evaluates the proportion of boundary pixels in the automatic segmentation that corresponds to the boundary pixels in the ground truth results. The precision and recall are computed as [38],

$$Precision = \frac{TP}{TP + FP} \tag{3.24}$$

$$Recall = \frac{TP}{TP + FN} \tag{3.25}$$

Lower precision value indicates over segmentation and lower recall value indicates under segmentation. The comparison of ground truth and segmentation algorithm can yield higher values of precision and recall if the boundaries of both segmentation results agree in location and level of details. Sometimes, the higher recall value might consider false positive and high precision value might miss some true annotations, therefore, the two measurements are combined to form a single unit known as F-score which is defined as the harmonic mean of precision and recall as,

$$F - score = \frac{2.Pricision.Recall}{Pricision + Recall} \tag{3.26}$$

3.6.1 Dice similarity coefficient

Dice similarity coefficient (DSC) measures similarity between the resulting and expected data sets. Let A be the resulting data set and B be the expected or ground truth data, then DSC is calculated as [40],

$$Dice(A, B) = 2.\frac{|A \cap B|}{|A| + |B|} \tag{3.27}$$

DSC computes spatial over index and reproducibility validation metric for two image sets. The value of DSC ranges from 0 to 1, indicating no spatial overlap to complete overlap between two sets of binary segmentation results.

3.6.2 Bland-Altman plots

Bland-Altman (B&A) plots also known as difference plots is a method of data plotting used in analyzing or correlating the agreement between two methods measuring same parameters [41]. B&A describes quantitative measurements by studying the mean difference and constructing limits of agreements with in 95% of the differences of the second method. The B&A is a scatter plot XY, where X axis shows the average of the both quantitative measure and Y axis shows the difference between the two measurements.

References

[1] Rupin Dalvi, Rafeef Abugharbieh, Mark Pickering, Jennie Scarvell, and Paul Smith, "Registration of 2d to 3d joint images using phase-based mutual information," in *Medical Imaging 2007: Image Processing*. International Society for Optics and Photonics, 2007, vol. 6512, p. 651209.

[2] Magnus Hemmendorff, Mats T Andersson, Torbjorn Kronander, and Hans Knutsson, "Phase-based multidimensional volume registration," *IEEE Transactions on Medical Imaging*, vol. 21, no. 12, pp. 1536–1543, 2002.

[3] Matthew Mellor and Michael Brady, "Phase mutual information as a similarity measure for registration," *Medical image analysis*, vol. 9, no. 4, pp. 330–343, 2005.

[4] Djamal Boukerroui, J Alison Noble, and Michael Brady, "On the choice of band-pass quadrature filters," *Journal of Mathematical Imaging and Vision*, vol. 21, no. 1-2, pp. 53–80, 2004.

[5] Ilker Hacihaliloglu, Rafeef Abugharbieh, Antony J Hodgson, and Robert N Rohling, "Bone surface localization in ultrasound using image phase-based features," *Ultrasound in medicine & biology*, vol. 35, no. 9, pp. 1475–1487, 2009.

[6] Ilker Hacihaliloglu, "Localization of bone surfaces from ultrasound data using local phase information and signal transmission maps," in *International Workshop and Challenge on Computational Methods and Clinical Applications in Musculoskeletal Imaging*. Springer, 2017, pp. 1–11.

[7] M Mary Synthuja Jain Preetha, L Padma Suresh, and M John Bosco, "Image segmentation using seeded region growing," in *Computing, Electronics and Electrical Technologies (ICCEET), 2012 International Conference on*. IEEE, 2012, pp. 576–583.

[8] Michael Felsberg and Ullrich Köthe, "Get: The connection between monogenic scale-space and gaussian derivatives," in *International Conference on Scale-Space Theories in Computer Vision*. Springer, 2005, pp. 192–203.

[9] Ilker Hacihaliloglu, Abtin Rasoulian, Robert N Rohling, and Purang Abolmaesumi, "Local phase tensor features for 3-d ultrasound to statistical shape+ pose spine model registration," *IEEE transactions on Medical Imaging*, vol. 33, no. 11, pp. 2167–2179, 2014.

[10] Michael Felsberg and Gerald Sommer, "The monogenic signal," *IEEE Transactions on Signal Processing*, vol. 49, no. 12, pp. 3136–3144, 2001.

[11] Ahror Belaid and Djamal Boukerroui, "α scale spaces filters for phase based edge detection in ultrasound images," in *Biomedical Imaging (ISBI), 2014 IEEE 11th International Symposium on*. IEEE, 2014, pp. 1247–1250.

[12] Athanasios Karamalis, Wolfgang Wein, Tassilo Klein, and Nassir Navab, "Ultrasound confidence maps using random walks," *Medical image analysis*, vol. 16, no. 6, pp. 1101–1112, 2012.

[13] Neeraj Sharma and Lalit M Aggarwal, "Automated medical image segmentation techniques," *Journal of medical physics/Association of Medical Physicists of India*, vol. 35, no. 1, pp. 3, 2010.

[14] Shilpa Kamdi and RK Krishna, "Image segmentation and region growing algorithm," *International Journal of Computer Technology and Electronics Engineering (IJCTEE) Volume*, vol. 2, 2012.

[15] Mohammed M Abdelsamea, "An enhancement neighborhood connected segmentation for 2d-cellular image," *arXiv preprint arXiv:1407.3664*, 2014.

[16] Regina Pohle and Klaus D Toennies, "Segmentation of medical images using adaptive region growing," in *Medical Imaging 2001: Image Processing*. International Society for Optics and Photonics, 2001, vol. 4322, pp. 1337–1347.

[17] Ferhat Bozkurt, Cemal Köse, and Ahmet San, "Comparison of seeded region growing and random walk methods for vessel and bone segmentation in cta images," in *Electrical and Electronics Engineering (ELECO), 2017 10th International Conference on*. IEEE, 2017, pp. 561–567.

[18] HP Ng, S Huang, SH Ong, KWC Foong, PS Goh, and WL Nowinski, "Medical image segmentation using watershed segmentation with texture-based region merging," in *Engineering in Medicine and Biology Society, 2008. EMBS 2008. 30th Annual International Conference of the IEEE*. IEEE, 2008, pp. 4039–4042.

[19] Jos BTM Roerdink and Arnold Meijster, "The watershed transform: Definitions, algorithms and parallelization strategies," *Fundamenta informaticae*, vol. 41, no. 1, 2, pp. 187–228, 2000.

[20] Chen Jia-xin and Liu Sen, "A medical image segmentation method based on watershed transform," in *Computer and Information Technology, 2005. CIT 2005. The Fifth International Conference on*. IEEE, 2005, pp. 634–638.

[21] Sébastien Lefèvre, "Knowledge from markers in watershed segmentation," in *International Conference on Computer Analysis of Images and Patterns*. Springer, 2007, pp. 579–586.

[22] Ghassan Hamarneh and Xiaoxing Li, "Watershed segmentation using prior shape and appearance knowledge," *Image and Vision Computing*, vol. 27, no. 1-2, pp. 59–68, 2009.

[23] Leo Grady, "Random walks for image segmentation," *IEEE transactions on pattern analysis and machine intelligence*, vol. 28, no. 11, pp. 1768–1783, 2006.

[24] Maxwell D Collins, Jia Xu, Leo Grady, and Vikas Singh, "Random walks based multi-image segmentation: Quasiconvexity results and gpu-based solutions," in *Computer Vision and Pattern Recognition (CVPR), 2012 IEEE Conference on*. IEEE, 2012, pp. 1656–1663.

[25] Ali Kemal Sinop and Leo Grady, "A seeded image segmentation framework unifying graph cuts and random walker which yields a new algorithm," in *Computer Vision, 2007. ICCV 2007. IEEE 11th International Conference on*. IEEE, 2007, pp. 1–8.

[26] Yuri Y Boykov and M-P Jolly, "Interactive graph cuts for optimal boundary & region segmentation of objects in nd images," in *Computer Vision, 2001. ICCV 2001. Proceedings. Eighth IEEE International Conference on*. IEEE, 2001, vol. 1, pp. 105–112.

[27] Daniel Freedman and Tao Zhang, "Interactive graph cut based segmentation with shape priors," in *null*. IEEE, 2005, pp. 755–762.

[28] Carsten Rother, Vladimir Kolmogorov, and Andrew Blake, "Grabcut: Interactive foreground extraction using iterated graph cuts," in *ACM transactions on graphics (TOG)*. ACM, 2004, vol. 23, pp. 309–314.

[29] MS Mallikarjuna Swamy and Mallikarjun S Holi, "Knee joint articular cartilage segmentation, visualization and quantification using image processing techniques: a review," *International Journal of Computer Applications (0975–8887) Volume*, 2012.

[30] Jurgen Fripp, Stuart Crozier, Simon K Warfield, and Sébastien Ourselin, "Automatic segmentation and quantitative analysis of the articular cartilages from magnetic resonance images of the knee," *IEEE transactions on medical imaging*, vol. 29, no. 1, pp. 55–64, 2010.

[31] S Kubilay Pakin, Jose Gerardo Tamez-Pena, Saara Totterman, and Kevin J Parker, "Segmentation, surface extraction, and thickness computation of articular cartilage," in *Medical Imaging 2002: Image Processing*. International Society for Optics and Photonics, 2002, vol. 4684, pp. 155–167.

[32] Stuart Solloway, Charles E Hutchinson, John C Waterton, and Christopher J Taylor, "The use of active shape models for making thickness measurements of articular cartilage from mr images," *Magnetic Resonance in Medicine*, vol. 37, no. 6, pp. 943–952, 1997.

[33] Calvin R Maurer, Rensheng Qi, and Vijay Raghavan, "A linear time algorithm for computing exact euclidean distance transforms of binary images in arbitrary dimensions," *IEEE Transactions on Pattern Analysis and Machine Intelligence*, vol. 25, no. 2, pp. 265–270, 2003.

[34] J Christopher Buckland-Wright, Diana G Macfarlane, John A Lynch, M Kris Jasani, and Charles R Bradshaw, "Joint space width measures cartilage thickness in osteoarthritis of the knee: high resolution plain film and double contrast macroradiographic investigation.," *Annals of the rheumatic diseases*, vol. 54, no. 4, pp. 263, 1995.

[35] Frank Heuer, Mark Sommers, JB Reid, and Michael Bottlang, "Estimation of cartilage thickness from joint surface scans: Comparative analysis of computational methods," *ASME-Publications-BED*, vol. 50, pp. 569–570, 2001.

[36] S Koo, GE Gold, and TP Andriacchi, "Considerations in measuring cartilage thickness using mri: factors influencing reproducibility and accuracy," *Osteoarthritis and cartilage*, vol. 13, no. 9, pp. 782–789, 2005.

[37] Matej Mlejnek, Anna Vilanova, and Meister Eduard Groller, "Interactive thickness visualization of articular cartilage," in *Proceedings of the conference on Visualization'04*. IEEE Computer Society, 2004, pp. 521–528.

[38] Fernando C Monteiro and Aurélio C Campilho, "Performance evaluation of image segmentation," in *International Conference Image Analysis and Recognition*. Springer, 2006, pp. 248–259.

[39] Jerrold T Bushberg and John M Boone, *The essential physics of medical imaging*, Lippincott Williams & Wilkins, 2011.

[40] Kelly H Zou, Simon K Warfield, Aditya Bharatha, Clare MC Tempany, Michael R Kaus, Steven J Haker, William M Wells III, Ferenc A Jolesz, and Ron Kikinis, "Statistical validation of image segmentation quality based on a spatial overlap index1: scientific reports," *Academic radiology*, vol. 11, no. 2, pp. 178–189, 2004.

[41] J Martin Bland, Douglas G Altman, et al., "Statistical methods for assessing agreement between two methods of clinical measurement," *lancet*, vol. 1, no. 8476, pp. 307–310, 1986.

Chapter 4

Results and Discussion

In this chapter, results and their interpretations on the cartilage segmentation and thickness computation from 2D US images are presented. In section 4.1, results and discussion on cartilage segmentation and thickness evaluation from enhanced B-mode US images using different region based segmentation algorithms are provided. The segmentation results are evaluated using DSC, precision, recall, and F-score metrics.

Both qualitative, and quantitative evaluations are performed to compare the segmentation results obtained by algorithms and performed manually by an expert on 200 data sets. The cartilage thickness measurement on a set of segmented images using proximity method is evaluated.

4.1 Cartilage segmentation

In this section, a comparison of different region based segmentation algorithms on enhanced B-mode US image and original B-mode US image is provided. In this framework, segmentation results were evaluated from RW, watershed, and graph-cut segmentation algorithms.

4.1.1 Cartilage segmentation qualitative results

The qualitative results of automatically extracted cartilage region using enhanced US image as input to the segmentation algorithm is shown in Figure 4.1, and Figure 4.2. The segmentation results depicts clear visualization of cartilage region from 2D US image. All the three segmentation algorithms yield satisfying results, while RW obtained results are better than watershed, and graph-cut.

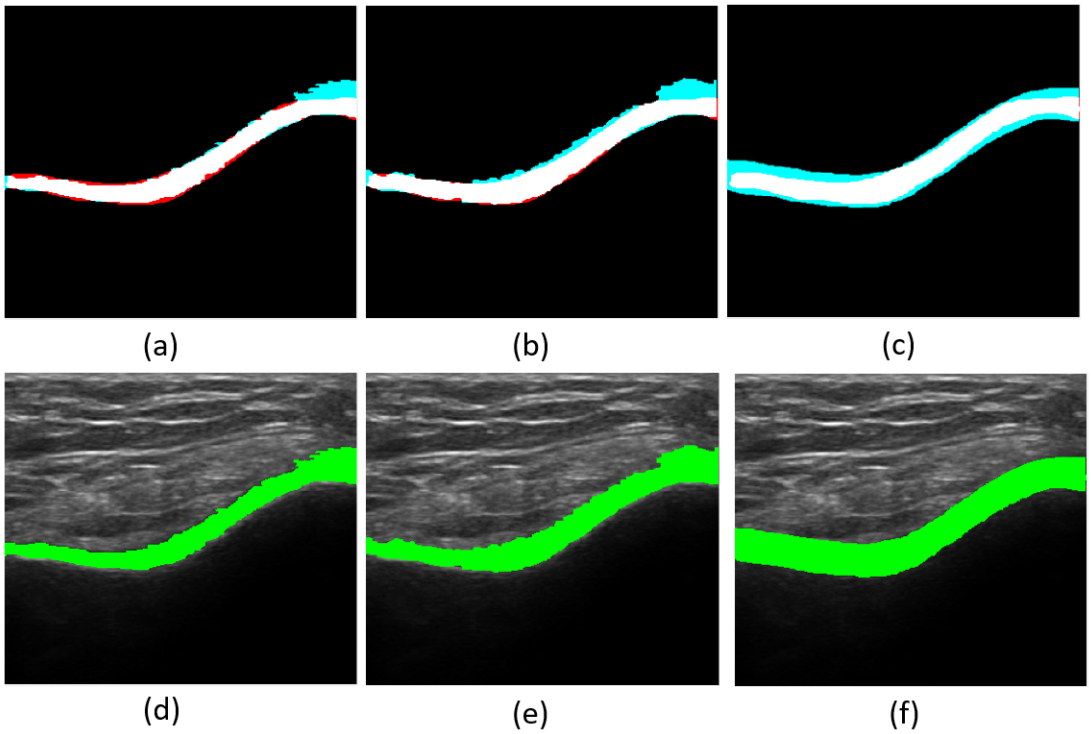

Figure 4.1: Qualitative results showing segmented cartilage from enhanced US image: Automatically segmented cartilage overlaid on the manual segmentation (Red: False negative, Cyan: False positive, White: Manually segmented cartilage): (a) Manual segmentation overlaid on RW. (b) Manual segmentation overlaid on watershed. (c) Manual segmentation overlaid on graph-cut. Segmented cartilage region overlaid on original B-mode US: (d) RW segmented cartilage overlaid on B-mode US. (e) Watershed segmented cartilage overlaid on B-mode US. (f) graph-cut segmented cartilage overlaid on B-mode US.

The qualitative results of automatically extracted cartilage region from original B-mode US images are shown in Figure 4.3. The qualitative results indicate, all the three segmentation algorithms yield the over segmentation of cartilage from the image and there is segmentation leak near the edges.

The qualitative results indicates the improved segmentation quality when using enhanced US image as an input to the segmentation methods.

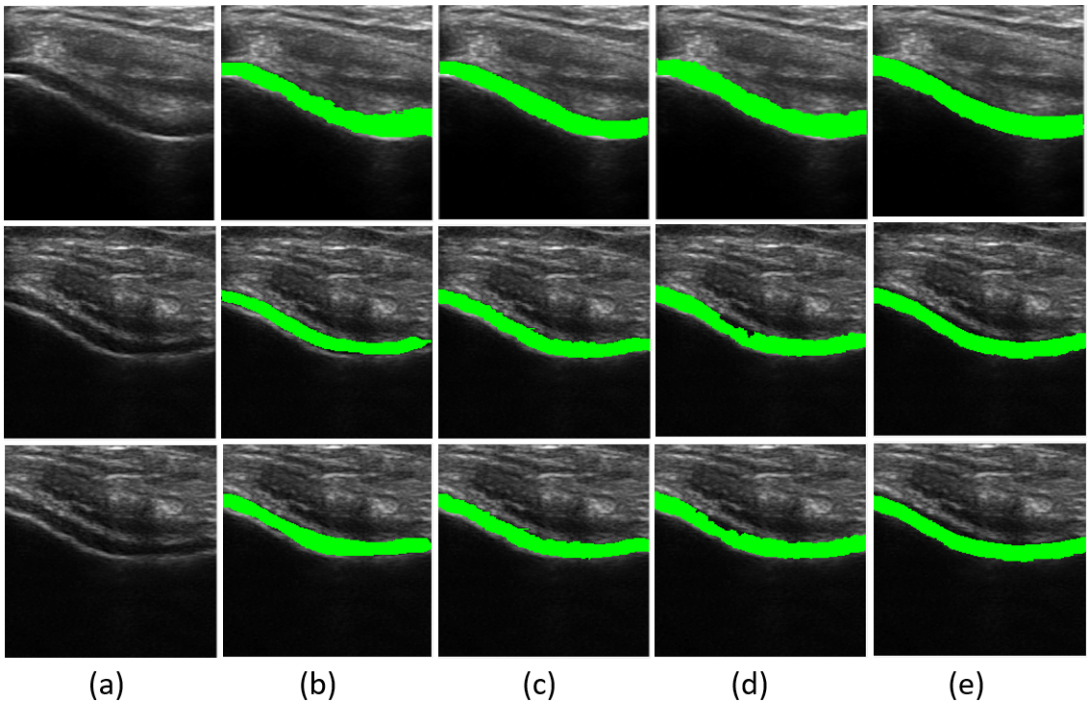

Figure 4.2: Segmented cartilage region overlaid on original B-mode US: Column (a) original B-mode US image. Column (b) Manually segmented cartilage overlaid on B-mode US. Column (c) RW segmented cartilage overlaid on B-mode US. Column (d) Watershed segmented cartilage overlaid on B-mode US. Column (e) Graph-cut segmented cartilage overlaid on B-mode US.

4.1.2 Cartilage segmentation quantitative results

The total computational time for segmentation using RW, watershed, and graph-cut are 11.08, 10.53, and 11.51 seconds respectively. Quantitative analysis were computed from the manual outline and the segmented cartilage region from total data sets of 200 images using DSC, precision, recall, and F-score metrics. Figure 4.4a, illustrate a quantitative comparison of RW, watershed, and graph-cut segmentation results validated using DSC values over the total data sets of 200 images using enhanced US images as an input to the segmentation methods. The figure shows, the computed DSC values ranged between 0.82 and 0.93, 0.70 and 0.93, and 0.76 and 0.89 for RW, watershed, and graph-cut respectively. The higher value of DSC metric indicates that the two comparing segmentation results have a good agreement in size and location, which correspond to

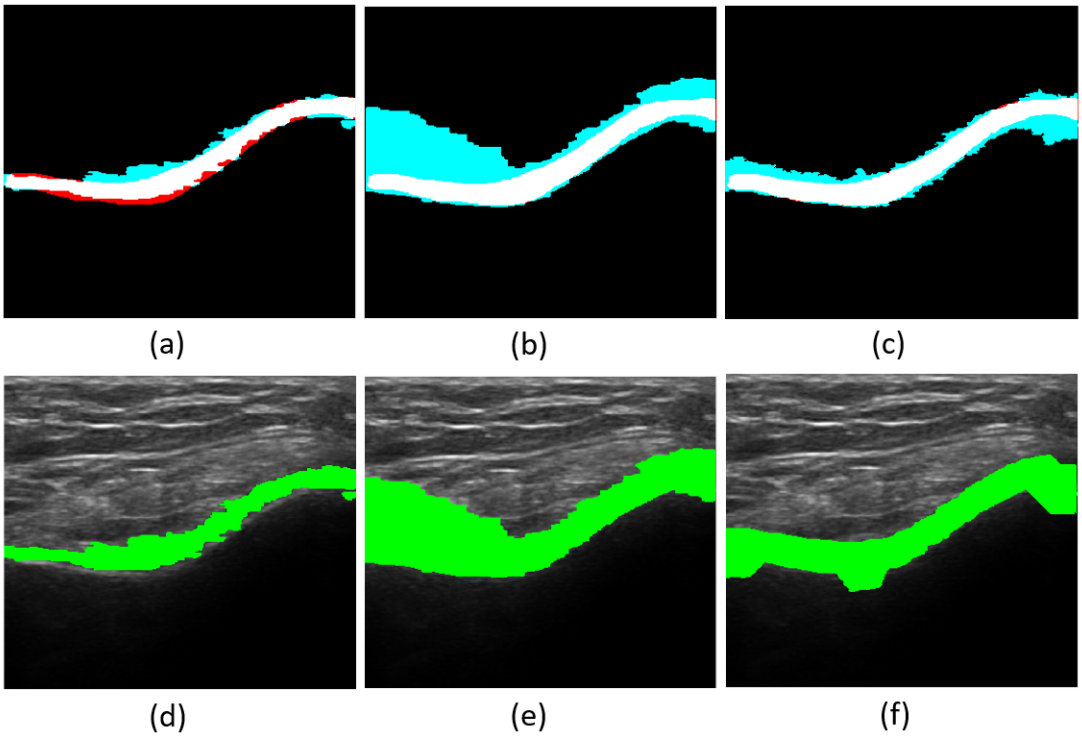

Figure 4.3: Qualitative results of cartilage segmentation on original B-mode US: Manual segmented cartilage overlaid on the automatically segmented by using (Red: False negative, Cyan: False positive, White: Manually segmented cartilage): (a) RW. (b) Watershed. (c) Graph-cut. Segmented cartilage region overlaid on original B-mode US: (d) RW segmented cartilage overlaid on B-mode US. (e) Watershed segmented cartilage overlaid on B-mode US. (f) graph-cut segmented cartilage overlaid on B-mode US.

more accurate segmentation results.

The mean and standard deviation of DSC, precision, recall, and F-score values for all the three methods over the total data sets of 200 images are summarized in Table 4.1, the mean DSC values were 0.90, 0.86, and 0.84 for RW, watershed, and graph-cut respectively. The table illustrates the satisfactory segmentation outcomes for all available data sets. The table indicates that RW segmentation algorithm, obtained higher average value for DSC metric for all available data sets than watershed and graph-cut.

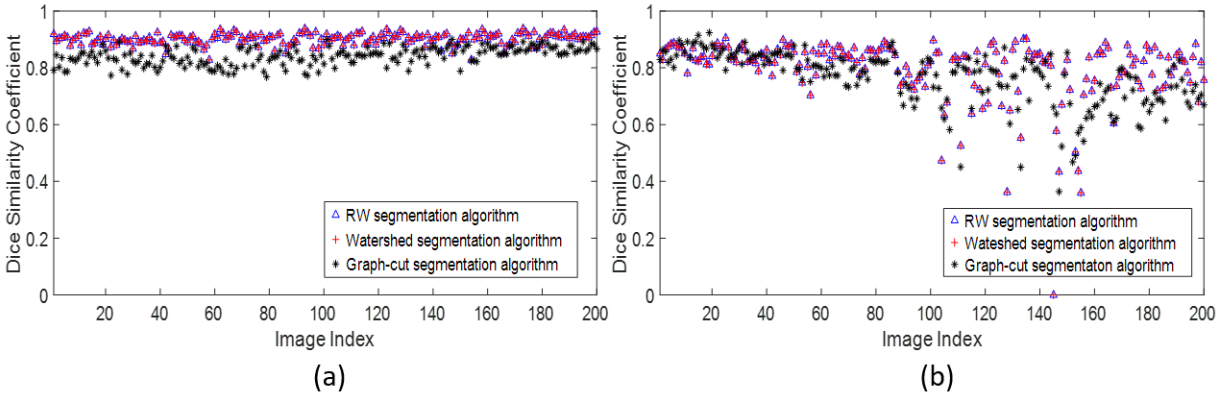

Figure 4.4: Dice similarity coefficient plots for comparison of segmentation algorithm with respect to manual segmentation. (a) DSC measures for different methods over a set of 200 B-mode US images evaluated using enhanced US images. (b) DSC measures for different methods over a set of 200 B-mode US images evaluated using original B-mode US images.

Table 4.1: Quantitative analysis using enhanced B-mode US images as the input to the segmentation methods.

Methods	DSC Mean ± SD	Precision	Recall	F-score
RW	0.90 ±0.01	0.88	0.92	0.90
Watershed	0.86 ± 0.04	0.82	0.91	0.86
Graph-cut	0.84 ± 0.03	0.81	0.87	0.84

The DSC values decreased to 0.79, 0.65, and 0.76 for RW, watershed, and graph-cut respectively when using original B-mode US images as an input to the segmentation methods (Table 4.2). The lower precision, and recall values indicates that the segmentation algorithm has returned less relevant values compared to the enhanced US images. Figure 4.4b, shows the distribution of DSC for segmentation algorithms over 200 original B-mode image. Investigating the plot, we can see that the region between image index values 90-200 have low DSC results due to the low contrast cartilage present in

the collected data (Figure 4.5). By comparing the quantitative analysis presented in Table 4.1 and 4.2, we can say that the cartilage segmentation using enhanced US images as an input to the segmentation method yields better accuracy, since our proposed enhancement method is intensity invariant, and it results in the enhancement of these low contrast scans and improves the segmentation accuracy for those scans.

Table 4.2: Quantitative analysis using original B-mode US images as the input to the segmentation methods.

Methods	DSC Mean ± SD	Precision	Recall	F-score
RW	0.79 ± 0.1	0.80	0.80	0.79
Watershed	0.65 ± 0.2	0.59	0.79	0.66
Graph-cut	0.76± 0.09	0.72	0.82	0.76

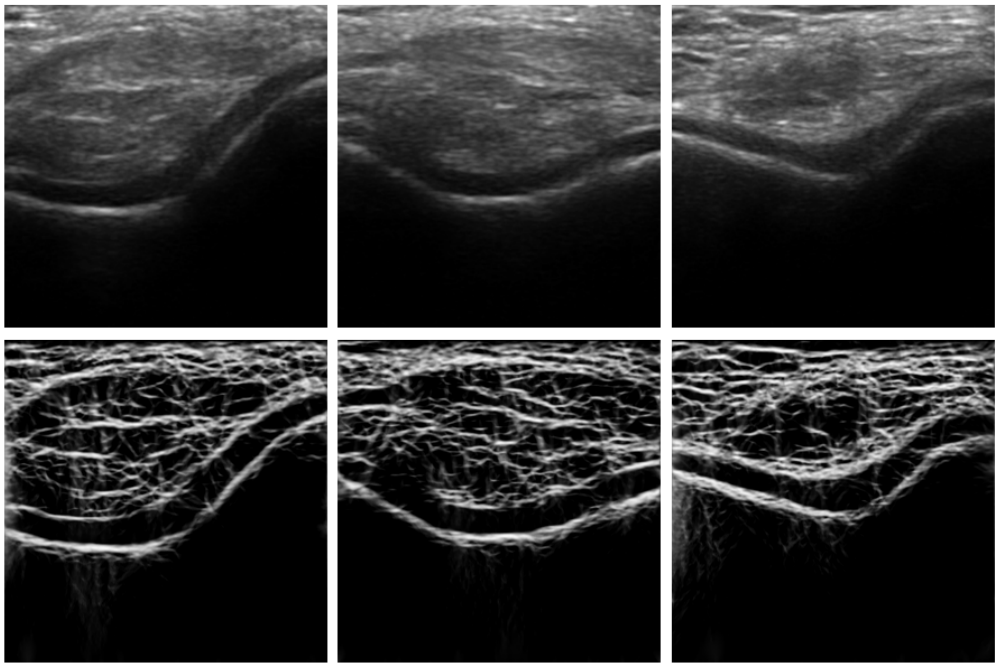

Figure 4.5: Example input images with poor DSC results. Top row shows the low contrast input images used in segmenting cartilage. Bottom row shows the enhanced cartilage bone surface used to evaluate segmentation result.

4.2 Cartilage thickness computation

The measured cartilage thickness ranged from 1.9 to 5.6. Table 4.3 shows the mean and standard deviation of average cartilage thickness obtained by manual measurement, automated measurement on segmented results obtained by manual, RW, watershed, and graph-cut methods. The results indicated by Table 4.3 shows the robustness of RW segmentation algorithm, to accurately locate and segment the cartilage region from the 2D US knee cartilage images. Quantitative results also indicate that there is a 0.15 mm difference between the thickness measurements obtained using manual landmark selection and manual segmentation. This is due to variation in manual measurements, which is expected as manual labeling of US data being an error prone procedure.

Table 4.3: Cartilage thickness measurement.

Method	Image	Mean ± SD (mm)
Manual measurement	Original B-mode	2.95 ± 0.66
Automated measurement	Manual Segmentation	3.1 ± 0.68
	RW	3.14 ± 0.46
	Watershed	3.23 ± 1.21
	Graph-cut	3.78 ± 0.35

The computed cartilage thickness measured by proximity method on segmented results obtained by RW, watershed, and graph-cut was compared using Bland-Altman (B/A) plots with the results obtained by manual thickness measurement on original B-mode US images. Figure 4.6, shows the B/A plots for thickness comparison between manually computed thickness and thickness computed on segmentation results obtained from RW, watershed, and graph-cuts. The mean error or the difference between the manual landmark thickness calculation all the pairs of thickness computations were -0.15 mm (±0.11 mm), -0.18 mm (±0.45 mm), -0.28 mm (±1.36 mm), and -0.83 mm (± 0.49 mm) for the manual segmentation, RW, watershed, and graph-cut methods respectively. The lower mean value depicts that there is no significant ply between the

two methods. The B/A plot indicates that most of the measured thickness difference lie within 95% limit of agreement i.e., 0.071 to -0.37, 0.69 to -1.07, 2.38 to -2.95, and 0.14 to -1.80 for manual/manual segmented, manual/RW, manual/watershed, and manual/graph-cut pair.

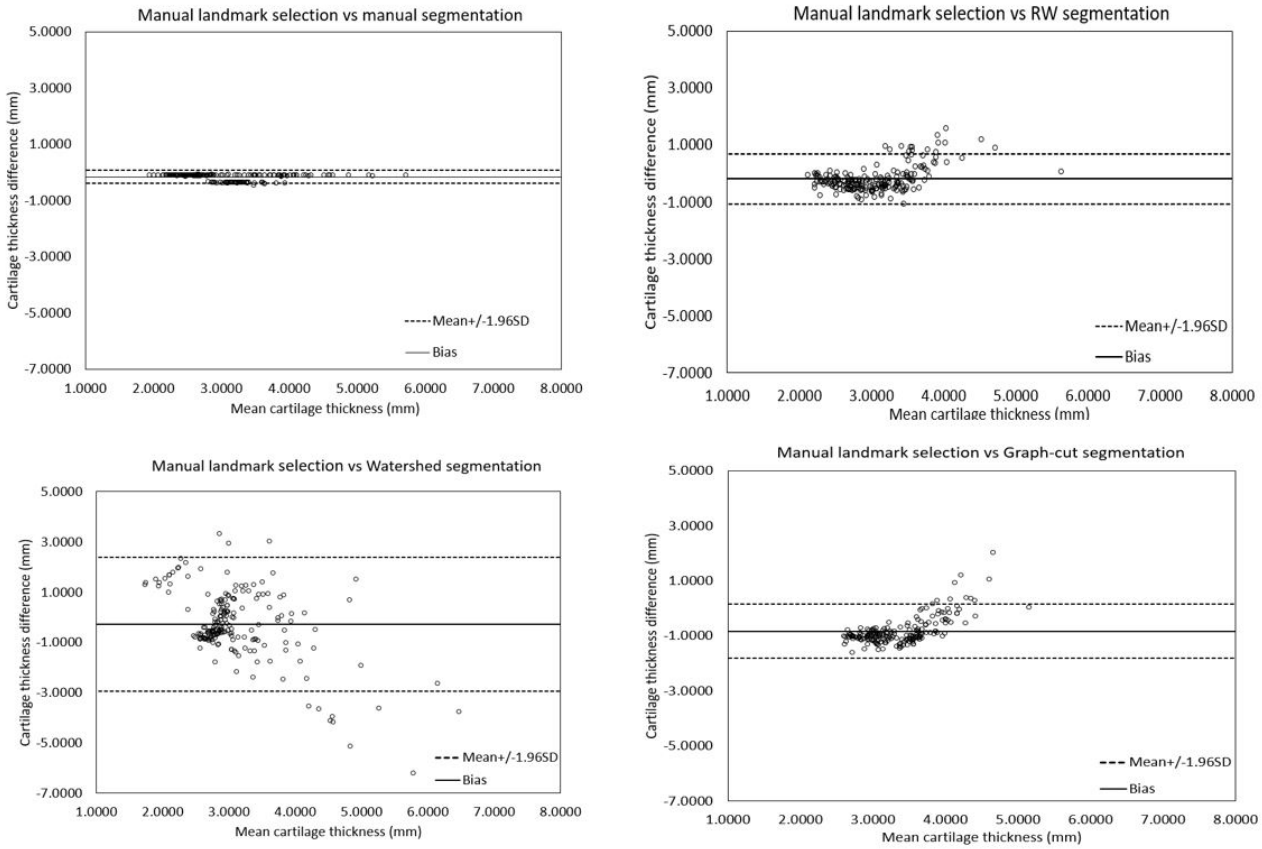

Figure 4.6: Bland-Altman plots for thickness comparison obtained by manual outline and thickness obtained using segmented cartilage region.

4.3 Discussion

The orientation of the transducer with respect to the imaged cartilage plane affects the appearance of the collected cartilage scans. The inclination of transducer may produce reduced contrast in the cartilage image, high levels of speckle noise, and limited visualization of bone surface. In this thesis, the 2D US knee cartilage were segmented with

and without enhancement. Without enhancement, the region based segmentation algorithm fails to properly distinguish the cartilage region from other surrounding tissues. The use of intensity invariant cartilage US image enhancement addresses the limitation of previously proposed intensity and gradient dependent enhancement methods.

In this thesis, the segmentation results from RW, watershed, and graph-cuts are evaluated. The qualitative and quantitative analysis indicates that among the three, RW shows more robustness and accurate results compared to expert manual segmentation. The performance of segmentation are evaluated using precision and recall. The lower recall value indicates under segmentation and lower precision value indicates over segmentation. Therefore, it is desired to have higher values for both precision and recall. RW segmentation algorithm has achieved 0.83 and 0.91 average precision and recall value which indicates that the segmentation algorithm has returned most relevant cartilage information. The comparison result of Bland-Altman plots thickness computation plot shows better agreement between thickness measured by RW segmentation results and manual measurement.

The validity of proposed method is compared with previously proposed MBORBHE cartilage enhancement method [2]. The histogram equalization based approach addressed the limitation of traditional HE by preserving the information of brightness shift, detail loss, and proper contrast enhancement, However, the framework also enhanced the soft tissue interface that is present in the 2D US image. Figure 4.7 shows the enhancement of cartilage region using proposed local phased feature method and MBORBHE. From the figure, it is evident that in HE based method, the soft tissues are enhanced greatly while in proposed method we can see a clear visualization of cartilage-bone interface.

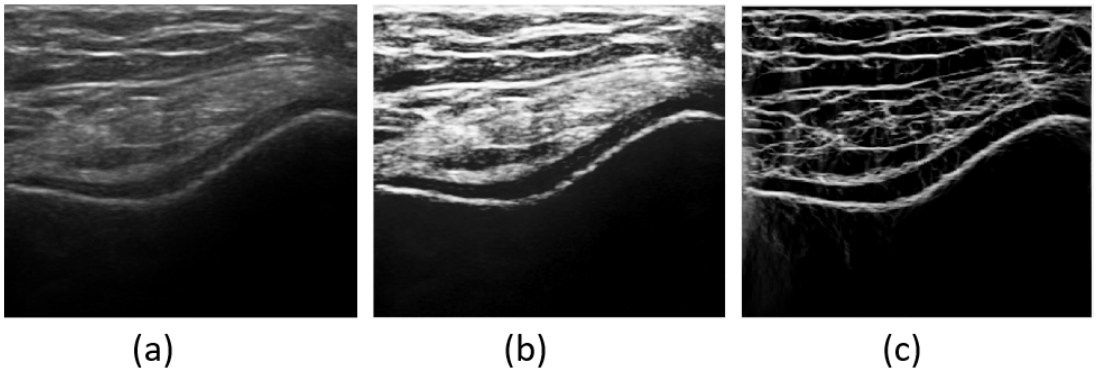

Figure 4.7: 2D US image enhancement. (a) original B-mode US image. (b) MBORBHE enhanced US image. (c) Proposed local phase based enhanced US image.

The HE enhanced US images were used to segment the cartilage. But the extracted bone surfaces were not continuous, due to the noise present in the image. The initial seeds for region based segmentation algorithm are shown in Figure 4.8. The broken seeds, failed to segment the cartilage region from 2D US images.

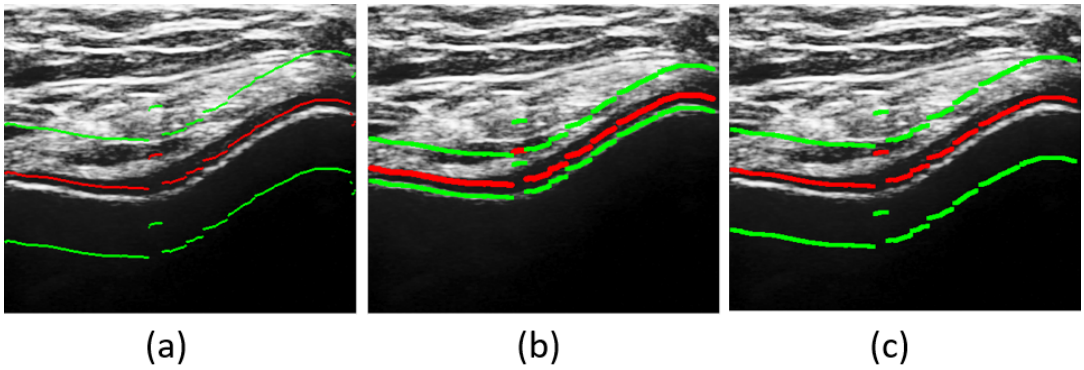

Figure 4.8: Seed Initialization on HE based enhanced US image (Red: Foreground seeds, Green: background seeds): (a) Foreground and background seeds RW segmentation algorithm. (b) Internal and external markers for watershed algorithm. (c) Foreground and background seeds for graph-cut algorithm.

In [3], the author proposed a segmentation algorithm using The locally statistical level set method (LSLSM). The obtained results showed the robustness of LSLSM method for cartilage segmentation. However, the method includes two user interactions

for initial contour initialization for cartilage boundary detection and extraction of cartilage regions from the surrounding soft tissue. The total computational time for LSLSM based segmentation algorithm was 13 seconds which is high for real time assessment.

The comparison with other previously proposed method indicate that, the framework presented in this thesis has potential application in determining cartilage degeneration.

References

[1] Esperanza Naredo, Carlos Acebes, Ingrid Möller, Fernando Canillas, Juan José de Agustín, Eugenio de Miguel, Emilio Filippucci, Annamaria Iagnocco, Carmen Moragues, Roser Tuneu, et al., "Ultrasound validity in the measurement of knee cartilage thickness," *Annals of the rheumatic diseases*, vol. 68, no. 8, pp. 1322–1327, 2009.

[2] Md Belayet Hossain, Khin Wee Lai, Belinda Pingguan-Murphy, Yan Chai Hum, Maheza Irna Mohd Salim, and Yih Miin Liew, "Contrast enhancement of ultrasound imaging of the knee joint cartilage for early detection of knee osteoarthritis," *Biomedical Signal Processing and Control*, vol. 13, pp. 157–167, 2014.

[3] Amir Faisal, Siew-Cheok Ng, Siew-Li Goh, and Khin Wee Lai, "Knee cartilage segmentation and thickness computation from ultrasound images," *Medical & biological engineering & computing*, vol. 56, no. 4, pp. 657–669, 2018.

Chapter 5

Conclusion and Future work

5.1 Conclusion

The cartilage segmentation and thickness computation method for the 2-D ultrasound images have been presented in this thesis. The performance of cartilage segmentation and thickness computation method have been evaluated qualitatively and quantitatively.

The 2D US knee cartilage segmentation using region based segmentation algorithms on local phase feature based enhanced US images have been proposed. The local phase cartilage enhancement is based on intensity invariant method which is used to enhance the cartilage-bone interface by suppressing the surrounding soft tissue interfaces. The enhanced cartilage images are used to aromatically extract the bone surface using US signal transmission maps and dynamic programming approach. The extracted bone surfaces are marked as initial seeds for the region based segmentation algorithm. The segmentation results from RW, watershed, and graph-cuts are evaluated and the qualitative and quantitative results are analyzed using DSC, precision, recall, and F-score metrics. The cartilage thickness is computed from segmented results using proximity approach. The thickness measured using each segmentation approach is compared to manually measured cartilage thickness using Bland-Altman plots. The framework presented in this thesis successfully addressed the limitation of US imaging modality in terms of low contrast and speckle noise and making US a valid modality for early screening and routine clinical monitoring of OA.

The segmentation results were computed using RW, watershed, and graph-cuts from US knee cartilage indicated that, the RW yielded better results than watershed and graph-cuts. The overall statistics of evaluation metrics of DSC, precision, recall, and

F-score indicates that RW has a consistent and good quality of segmentation results for the overall data set of images. The computed cartilage thickness on segmented cartilage indicates the agility, reproducibility, and agreement of the segmentation algorithm in segmenting various cartilage thickness.

The possibility of cartilage segmentation and thickness computation from 2D US knee images using proposed method directs the potential application of the method for the assessment and analysis knee cartilage degradation in US images. The proposed method can be used to evaluate cartilage degeneration by assessing cartilage thickness quantified over a particular time duration by comparing the cartilage thickness at certain time interval to have a better treatment plan to treat long term OA.

5.2 Limitations

The important consideration for the proposed cartilage segmentation using region based algorithm is the placement of initial seeds. The segmentation algorithm is sensitive to the initial seeds, here the seeds are placed based on prior knowledge of cartilage shape. Therefore, selecting an accurate and optimized placement of seeds. In this experiment, no OA images have been used for the segmentation, therefore, a rigorous analysis is needed on OA knee cartilage scans. The average computational time for the framework is 11 sec, which can cause delay in real time processing. The future work will include optimization of framework, to decrease the processing time.

5.3 Future work

The presented framework in this thesis can be extended to various studies for early detection and classification of OA as described below.

5.3.1 Assessment of degree of cartilage degeneration

The proposed method has shown its validity to effectively measure the cartilage thickness. The computed cartilage thickness is useful to classify the cartilage as normal, and pathological OA cartilage using expert knowledge. We can generate cartilage grading

system for OA, based on the degree of degeneration as normal to severe. The change in cartilage thickness ca be assessed over the time at a certain time interval. As OA is slow progressive disease, cartilage degradation might occur after a long time therefore, monitoring the occurrence need follow up scans over time.

5.3.2 Assessment of tracked ultrasound volume for increased field of view

The 2D US knee cartilage segmentation and thickness computation are limited to a specific plane of view obtained by the 2-D ultrasound probe. The field of view (FOV) of US depends on the transducer width. To increase the FOV, and to have better visualization of cartilage region through medial and lateral condyle, we can use tracked volume. This provides the visualization of cartilage from axial, lateral, and sagittal plane. The segmented results can be used to reconstruct 3D model of cartilage.

5.3.3 Assessment of ultrasound image using deep learning segmentation algorithm

The proposed work can be extended to segment the US knee images using deep learning algorithms on more data sets collected from subjects with different age group, gender, including OA knee images.

5.3.4 Comparison of cartilage thickness between ultrasound and magnetic resonance imaging

There is no proper comparison available between the cartilage thickness measured using US and MRI. This study can be extended to compare the cartilage thickness measured using proposed method with that of cartilage thickness computed from MRI. The comparison results can indicate the accuracy and validity of US for screening knee OA.

List of publications

1. Prajna Ramesh Desai and Ilker Hacihaliloglu, "Enhancement and automated segmentation of ultrasound knee cartilage for early diagnosis of knee osteoarthritis," in Biomedical Imaging (ISBI 2018), 2018 IEEE 15th International Symposium on. IEEE, 2018, pp. 1471-1474

Appendix A: Ethics approval letter

RUTGERS
THE STATE UNIVERSITY OF NEW JERSEY

Office of Research and Regulatory Affairs
Arts and Sciences IRB
Rutgers, The State University of New Jersey
335 George Street / Liberty Plaza / Suite 3200
New Brunswick, NJ 08901

https://orra.rutgers.edu/hspp

732-235-2866

April 14, 2017

Ilker Hacihaliloglu
599 Taylor Rd
Piscataway NJ 08854

P.I. Name: Hacihaliloglu
Protocol #: 15-561M

Dear Ilker Hacihaliloglu:

Initial	Amendment	Continuation	Continuation w/ Amend	Adverse Event
		✓		

Protocol Title: "Computer Assisted Orthopedic Surgery Using 3D Ultrasound Imaging"

This is to advise you that the above-referenced study has been presented to the Institutional Review Board for the Protection of Human Subjects in Research, and the following action was taken subject to the conditions and explanations provided below:

Approval Date: 4/14/2017 **Expiration Date:** 4/13/2018 **Expedited Category(s):**1,4
Approved # of Subject(s): 100 **Currently Enrolled:** 5

This approval is based on the assumption that the materials you submitted to the Office of Research and Sponsored Programs (ORSP) contain a complete and accurate description of the ways in which human subjects are involved in your research. The following conditions apply:

- **This Approval-**The research will be conducted according to the most recent version of the protocol that was submitted. **This approval is valid ONLY for the dates listed above;**
- **Reporting-**ORSP must be immediately informed of any injuries to subjects that occur and/or problems that arise, in the course of your research;
- **Modifications-**Any proposed changes MUST be submitted to the IRB as an amendment for review and approval prior to implementation;
- **Consent Form(s)-**Each person who signs a consent document will be given a copy of that document, if you are using such documents in your research. The Principal Investigator must retain all signed documents for at least three years after the conclusion of the research;
- **Continuing Review-**You should receive a courtesy e-mail renewal notice for a Request for Continuing Review before the expiration of this project's approval. However, it is your responsibility to ensure that an application for continuing review has been submitted to the IRB for review and approval prior to the expiration date to extend the approval period;

Additional Notes:
- **Continuation Expedited Approval per 45 CFR 46.110.**

Failure to comply with these conditions will result in withdrawal of this approval.
Please note that the IRB has the authority to observe, or have a third party observe, the consent process or the research itself. The Federal-wide Assurance (FWA) number for the Rutgers University IRB is FWA00003913; this number may be requested on funding applications or by collaborators.

Respectfully yours,

Acting For--
Beverly Tepper, Ph.D.
Professor, Department of Food Science
IRB Chair, Arts and Sciences Institutional Review Board
Rutgers, The State University of New Jersey

(GJ:hb)

RUTGERS
THE STATE UNIVERSITY OF NEW JERSEY

RE: Participation request for Computer Assisted Orthopedic Surgery Using 3D Ultrasound Imaging Study

Rutgers University, School of Engineering, Department of Biomedical Engineering is conducting a study to demonstrate the clinical feasibility of using ultrasound for imaging bone surfaces in orthopaedic surgery applications. The main imaging modality which is going to be used in this study is Ultrasound. Ultrasound is a well-established imaging modality in medicine, which has no known risks and involves no ionizing radiation.

Subjects who are Biomedical Engineering students are invited to participate in this study. The study will involve placing gel over the anatomical area (femur, tibia, knee, pelvis and spine) area and scanning with Ultrasound probe from different angles.

We would appreciate your participation in this study. If you are interested in participating or for more information, please contact Dr. Ilker Hacihaliloglu at +1 848-445-6564 or ilker.hac@rutgers.edu .

Yours sincerely,

Dr. Ilker Hacihaliloglu

Principal Investigator
Dept of Biomedical Engineering

Cosmas Mwikirize

Co-Investigator
(Graduate Student)
Dept of Biomedical Engineering

APPROVED
APR 14 2017
Approved by the Rutgers IRB

EXPIRES
APR 13 2018
Approved by the Rutgers IRB

RUTGERS

Office of Research and Regulatory Affairs
Arts and Sciences IRB
Rutgers, The State University of New Jersey
335 George Street / Liberty Plaza / Suite 3200
New Brunswick, NJ 08901

orra.rutgers.edu/artsci

732-235-2866

June 13, 2018

Ilker Hacihaliloglu
599 Taylor Rd
Piscataway NJ 08854

P.I. Name: Hacihaliloglu
Protocol #: 15-661M

Dear Ilker Hacihaliloglu:

Initial	**Amendment**	✓ **Continuation**	**Continuation w/ Amend**	**Adverse Event**

Protocol Title: "Computer Assisted Orthopedic Surgery Using 3D Ultrasound Imaging"

This is to advise you that the above-referenced study has been presented to the Institutional Review Board for the Protection of Human Subjects in Research, and the following action was taken subject to the conditions and explanations provided below:

Approval Date: 4/4/2018 **Expiration Date:** 4/3/2019
Expedited Category(s): 1,4 **Approved # of Subject(s):** 100 **Currently Enrolled:** 17

This approval is based on the assumption that the materials you submitted to the Office of Research and Sponsored Programs (ORSP) contain a complete and accurate description of the ways in which human subjects are involved in your research. The following conditions apply:

- **This Approval-**The research will be conducted according to the most recent version of the protocol that was submitted. **This approval is valid ONLY for the dates listed above;**
- **Reporting-**Reporting- Reporting—ORRA/Arts & Sciences IRB must be immediately informed of any injuries to subjects that occur (within 24 hours) and/or problems (e.g., subject complaints) that arise, in the course of your research within a timely manner (within 5 business days). Visit our website for more information on reportable events, https://orra.rutgers.edu/reportable-events.
- **Modifications-**Any proposed changes MUST be submitted to the IRB as an amendment for review and approval prior to implementation;
- **Consent Form(s)-**Each person who signs a consent document will be given a copy of that document, if you are using such documents in your research. The Principal Investigator must retain all signed documents for at least three years after the conclusion of the research;
- **Continuing Review-**You should receive a courtesy e-mail renewal notice for a Request for Continuing Review before the expiration of this project's approval. However, it is your responsibility to ensure that an application for continuing review has been submitted to the IRB for review and approval prior to the expiration date to extend the approval period;

Additional Notes:
- **Continuation Expedited Approval per 45 CFR 46.110**

Failure to comply with these conditions will result in withdrawal of this approval.
Please note that the IRB has the authority to observe, or have a third party observe, the consent process or the research itself. The Federal-wide Assurance (FWA) number for the Rutgers University IRB is FWA00003913; this number may be requested on funding applications or by collaborators.

Respectfully yours,

Michelle Matthews

Acting For--
Beverly Tepper, Ph.D.
Professor, Department of Food Science
IRB Chair, Arts and Sciences Institutional Review Board
Rutgers, The State University of New Jersey

(MW:wbc)

Appendix B: Elsevier license for Figure 1.2

ELSEVIER LICENSE
TERMS AND CONDITIONS

Jul 26, 2018

This Agreement between Ms. Prajna Desai ("You") and Elsevier ("Elsevier") consists of your license details and the terms and conditions provided by Elsevier and Copyright Clearance Center.

License Number	4396591444346
License date	Jul 26, 2018
Licensed Content Publisher	Elsevier
Licensed Content Publication	Osteoarthritis and Cartilage
Licensed Content Title	Diagnostic performance of knee ultrasonography for detecting degenerative changes of articular cartilage
Licensed Content Author	S. Saarakkala,P. Waris,V. Waris,I. Tarkiainen,E. Karvanen,J. Aarnio,J.M. Koski
Licensed Content Date	May 1, 2012
Licensed Content Volume	20
Licensed Content Issue	5
Licensed Content Pages	6
Start Page	376
End Page	381
Type of Use	reuse in a thesis/dissertation
Portion	figures/tables/illustrations
Number of figures/tables/illustrations	1
Format	electronic
Are you the author of this Elsevier article?	No
Will you be translating?	No
Original figure numbers	Figure 2
Title of your thesis/dissertation	Enhancement and automated segmentation of ultrasound knee cartilage for early diagnosis of knee osteoarthritis
Expected completion date	Aug 2018
Estimated size (number of pages)	70
Requestor Location	Ms. Prajna Desai 5 McEvoy R EDISON, NJ 08837 United States Attn: Ms. Prajna Desai
Publisher Tax ID	98-0397604
Total	0.00 USD
Terms and Conditions	